City Research Online

City, University of London Institutional Repository

This is the accepted version of the paper.

This version of the publication may differ from the final published version.

Variable Spaced Particle in Meshfree Method to handle wave-floating body interactions

A.S. Rijas[1], V. Sriram[1*] and S.Yan[2]

[1]Department of Ocean Engineering, IIT Madras, Chennai, India.

[2]School of Engineering and Mathematical Sciences, City University of London, Northampton Square, London, UK

*vsriram@iitm.ac.in

ABSTRACT

In this work, the motion of a 2D rectangular freely floating body under waves is simulated using Improved Meshless Local Petrov-Galerkin method based on Rankine Source function (IMLPG_R) with variable spacing resolutions. The IMLPG_R method is a particle method which solves Navier-Stokes equations using the fractional step method to capture the wave properties. However, many existing particle methods are computationally intensive to model the wave-floating body due to the requirement of fine particles, needing uniform distribution throughout the domain. In order to improve the computational efficiency and capture the body response properly, variable spaced particle distribution with fine resolution near the floating body and coarse resolution far from the body is implemented. Numerical schemes to handle variable resolutions are reported. An iterative scheme to handle the wave floating body is implemented in the particle method. Two test cases, one with small wave and another with steep waves are simulated for uniform particle distribution and the result shows good agreement with literature. Based on this, the performance of the variable spaced particle distribution is tested in coupling with floating body solver. The application of the method for wave impact load from the green water loading of the floating structure is also simulated.

1 INTRODUCTION

Wave interaction with the floating body is a traditional research topic in the field of naval architecture and offshore engineering. Concerning the safety and the operation of these structures in these fields, the prediction of the dynamic behaviour of the body under wave excitation is very important. The experimental investigation has lots of limitation due to time and cost. So, the computational methods are preferred for performing wave floating structure interaction. The complexity of solving the equation of motion of the floating body and fluid particle movement simultaneously is the major challenge in the computational method.

The modelling of numerical wave tank (NWT) for the simulation of wave floating structure interaction problem uses two approaches: one is fully nonlinear potential flow theory (FNPT) models and another one is Navier-Stokes model (NS). The early developed FNPT models are not suitable for modelling the fluid if breaking wave impacts, viscosity and turbulent effects are

significant. So Navier-Stokes equations together with continuity equations are used to model fluid part of fluid-structure interaction problems for these issues. Three types of formulations have been proposed for the NS model: Eulerian, Lagrangian and Arbitrary Lagrangian-Eulerian (ALE) formulations. Different numerical methods such as Finite Difference Method (FDM) and Finite Volume Method (FVM) are used to discretize the fluid domain in the Eulerian grid-based formulation of Navier Stokes equations. Even though the mesh-based NS models will produce impressive results, its success widely depends on the quality of the mesh/grid. This makes the modelling of fluid using the Navier Stokes equation a time-consuming task. The difficulties associated with Eulerian grid formulation can be overcome by Lagrangian formulation using mesh-free or particle-based method. The mesh-free method discretizes the problem domain into randomly distributed nodes with no interconnectivity as in mesh-based methods.

Various particle methods reported in the literature are Diffusion Element Method [1], Element Free Galerkin method [2], Smoothed Particle Hydrodynamics [3], Reproducing Kernel Particle method [4], Moving Particle Semi-implicit method [5] etc. Amongst Smoothed Particle Hydrodynamics (SPH) and Moving Particle Semi-implicit (MPS) method is the usual method for solving water wave problems[6]. Generally, these particle methods are grouped into weakly compressible and incompressible particle method. Weakly compressible particle method solves the equation of state to estimate the pressure, whereas the incompressible particle method solves the pressure Poisson equation to calculate the pressure.

The first work in wave interaction with the floating body using particle method has been performed by Koshizuka et al[7] using MPS method in 1998. In this work, they simulated breaking wave interaction with a floating body. Sueyoshi [8] performed the motion of a 2D rectangular floating body under waves using MPS method. The influence of water on the deck to the motion of a floating body has been simulated by Sueyoshi et al [9] by applying MPS. The MPS method is used by Ikari et al[10] to predict the mooring force acting on a floating body. The violent wave - 2D rectangular floating body interactions with an inner liquid tank has been simulated by Lee et al [11] and the wave interaction with the free-rolling body is done by Zhang et al[12] using MPS method. All the above MPS methods use the pressure Poisson equation for pressure estimation.

In SPH, the first simulation for fluid-solid coupling was done by Monaghan and Kos [13] in 2000. Monaghan et al [14] studied the water entry of a rectangular rigid body sliding down a slope by using WCSPH method. WCSPH simulation of water entry of different types of free falling bodies has been done by Doring et al [15], Oger et al[16] and Ulrich et al [17]. Hashemi et al [18] performed falling of two circular cylinders through a vertical channel and Canelas et al [19] modelled rising as well as sinking of a circular cylinder in water using WCSPH method. Bouscasse et al[20] adopted WCSPH method to study the response of rectangular floating body under wave packets and Ren et al[21] also adopted WCSPH method to predict the motion of freely floating body in waves. In order to improve the efficiency of WCSPH method, Omidvar et al [22,23] introduced variable particle mass technique, which reduces the computation effort by reducing the number of particles in the fluid domain. The ISPH method for wave-float interaction was developed by Zheng et al[24].

The above literature clearly shows that most of the researches in particle method have been carried out either on different motions of floating bodies in calm water or the wave interaction with floating body with motion restricted in some direction. The investigations related to the motion of the floating body with combination of sway, heave and roll under wave with a smaller number of particles are rare. The present work aims to simulate the 2D wave interaction with the freely floating body using the recently developed mesh-free method called IMLPG_R (Improved Meshless Local Petrov-Galerkin method with Rankine source function) method with variable particle distribution.

The MLPG method was first introduced by Atluri and Zhu [25], which solves the partial differential equations by using the local weak form and the local approximation of unknown variables are doing by using Moving Least Square (MLS) method. Lin and Atluri [26] adopted this MLPG method to solve Navier-Stokes (NS) equations. Ma [27] applied this MLPG method for modelling nonlinear water waves. This method uses the pressure Poisson equation to estimate pressure. Ma [28,29] altered this MLPG method to a new form termed MLPG_R (Meshless Local Petrov-Galerkin method with Rankine source function) by applying two changes in methodology, (i) replaced Heaviside step function with Rankine source function as test function to formulate the weak form over local sub-domains, which enhances the accuracy and stability of the pressure calculation by producing a weak form of governing equations, that did not contain the gradients of unknown variables (ii) developed the Simplified Finite Difference Interpolation (SFDI), which do not need the inverse calculation of matrix, to accelerate the interpolation and gradient estimation. Ma and Zhou [30] used this MLPG_R method to simulate 2D breaking waves. Sriram and Ma[31] further modified this MLPG_R method to IMLPG_R (Improved MLPG_R) method for modelling wave interaction with elastic structures, in which new scheme is imposed for better accuracy of pressure gradient computation. Divya and Sriram [32] applied this IMLPG_R method to wave-porous structure interaction problem. The IMLPG_R method is further extended to simulate forced heave oscillation of 2D rectangular floating body on the free surface of a viscous fluid by Rijas and Sriram [33] and to perform the free roll decay as well as free heave decay test of the 2D rectangular floating body by Rijas et al [34]. Our previous works simulated only the single degree of freedom problem of floating body on the free surface of the calm water. This will be the first paper simulating the interaction of the nonlinear wave with the freely floating body using the IMLPG_R method. In order to improve the computational efficiency, variable spaced particle distribution is implemented, in which high resolution of particle distribution is used near the floating body and low-resolution particle distribution is applied in the far field from the floating body and developed the scheme wherein it can be used effectively.

The paper is arranged in the following manner. Starting with mathematical modelling of the governing equations using the IMLPG_R method, then floating body modelling, free surface identification technique and variable particle distribution method are discussed. In the results and discussion part, convergence and validation test are performed with uniform particle distribution. Then the simulation has been reported for variable particle distribution and comparison with uniform particle distribution is carried out. Finally, the new variable spaced particle domain is used to simulate green water loading of the floating body.

2 MATHEMATICAL MODEL

2.1 Governing equations and boundary conditions

The 2D incompressible Navier-Stokes equations and continuity equations along with proper boundary conditions are used to describe the fluid motion of the wave-floating body interaction problem in this work. The mass and momentum conservation equations in Lagrangian form can be represented as

$$\nabla . \vec{u} = 0 \tag{1}$$

$$\frac{D\vec{u}}{Dt} = -\frac{1}{\rho}\nabla p + \vec{g} + \upsilon\nabla^2\vec{u} \tag{2}$$

where $\vec{u}$ is the fluid particle velocity, p is the particle pressure, ρ is the fluid density, υ is the kinematic viscosity of the fluid and $\vec{g}$ is the gravitational acceleration. The kinematic and dynamic free surface boundary conditions are expressed as

$$\frac{D\vec{r}}{Dt} = \vec{u} \tag{3}$$

$$p = 0 \tag{4}$$

where $\vec{r}$ is the position vector. The boundary conditions for solid boundaries including floating body surface are

$$\vec{u}.n = \vec{U}.n \tag{5}$$

$$\vec{n}.\nabla p = \rho\left(\vec{n}.\vec{g} - \vec{n}.\dot{\vec{U}} + \upsilon\vec{n}.\nabla^2\vec{u}\right) \tag{6}$$

where $\vec{U}$ and $\dot{\vec{U}}$ are the velocity and acceleration of the solid boundary particles respectively and $\vec{n}$ is the unit normal vector to the solid boundary.

2.2 Numerical procedure

In the IMLPG_R method, the fractional time-split algorithm proposed by Chorin [35] is used to solve the above equations. The steps are as following:

i. Explicitly find out the intermediate velocity $\vec{u}^*$ and position $\vec{r}^*$ of the particles using

$$\vec{u}^* = \vec{u}^n + \vec{g}\Delta t + \upsilon\nabla^2\vec{u}^n\Delta t \tag{7}$$

$$\vec{r}^* = \vec{r}^n + \vec{u}^*\Delta t \tag{8}$$

where superscript 'n' denotes n^{th} time step and 'Δt' is the time step size.

ii. Implicitly evaluate pressure p^{n+1} from the pressure Poisson equation [30] given by:

$$\nabla^2 p^{n+1} = \alpha\frac{\rho^{n+1} - \rho^*}{\Delta t^2} + (1-\alpha)\frac{\rho}{\Delta t}\nabla . \vec{u}^* \tag{9}$$

where 'α' is an artificial coefficient between 0 and 1, and ρ^{n+1} and ρ^* is fluid density at $(n+1)^{th}$ time step and intermediate time step, respectively. The value of 'α' is taken as zero by Sriram and Ma [31] for their IMLPG_R method.

iii. Update the fluid particle velocity and position at $(n+1)^{th}$ time step using

$$\vec{u}^{n+1} = \vec{u}^* - \frac{\Delta t}{\rho} \nabla p^{n+1} \tag{10}$$

$$\vec{r}^{n+1} = \vec{r}^* + u^{n+1} \Delta t \tag{11}$$

2.3 IMLPG_R formulation

In the above-described algorithm, the key task is to solve the pressure Poisson equation. In this work, the IMLPG_R method is adopted to solve the pressure Poisson equation. If $\alpha=0$, the Eq.9 can be written as

$$\nabla^2 p^{n+1} = \frac{\rho}{\Delta t} \nabla.\vec{u}^* \tag{12}$$

The meshless method discretizes the computational domain into randomly distributed particles or nodes. Each particle I in the domain is enclosed by a circular sub-domain Ω_I centred at the node itself, having radius R_I. The weak form of Eq.12 is obtained by multiplying it with an arbitrary test function φ and integrating over the circular sub-domain of each particle. The test function used in the IMLPG_R method is the solution of Rankine source function, i.e. $\varphi = \frac{1}{2\pi} \ln(r/R_I)$ [28], r is the distance between surrounding particle inside the sub-domain and centre I of the sub-domain. So Eq.12 becomes

$$\int_{\Omega_I} \left[\nabla^2 p - \frac{\rho}{\Delta t} \nabla.\vec{u}^* \right] \varphi d\Omega = 0 \tag{13}$$

In order to avoid the numerical calculation of gradients and derivatives in the above equation, a zero term $p\nabla^2\varphi$ is added to Eq.13 and Gauss theorem is applied, which leads to the final form as,

$$\int_{S_I} n.(p\nabla\varphi)ds - p = \int_{\Omega_I} \frac{\rho}{\Delta t} \vec{u}^*.\nabla\varphi d\Omega \tag{14}$$

where S_I is the boundary of the subdomain Ω_I. Similarly, Eq.6 is modified by combining with Eq.5 and Eq.10 into a new form as shown below

$$n.\nabla p^{n+1} = \frac{\rho}{\Delta t} n.\left(\vec{u}^* - \vec{U}^{n+1}\right) \tag{15}$$

The pressure in the left-hand side of Eq.14 is interpolated by using the MLS method and integration on the right-hand side is executed by the semi-analytical method. More details about discretization of Eq.14 and Eq.15 are given in [28],[29]&[30], and the same will not be repeated here, only the final equation is given below.

$$\mathbf{K_{ij}.P = B_i} \tag{16}$$

where,

$$P(\vec{x}) = \sum_{j=1}^{N} \Phi_j(\vec{x}) \hat{p}_j$$

$$K_{ij} = \begin{cases} \iint_{S_I} \Phi_j(\vec{x}) n.\nabla\varphi ds - \Phi_j(\vec{x}_i) & \text{for inner nodes} \\ n.\nabla\Phi_j(\vec{x}_i) & \text{for solid boundary nodes} \end{cases}$$

and

$$
B_i = \begin{cases} \int_{\Omega_I} \dfrac{\rho}{\Delta t} u^* . \nabla \varphi d\Omega & \text{for inner nodes} \\[2ex] \dfrac{\rho}{\Delta t} n.\left(\vec{u}^* - \vec{U}^{n+1}\right) & \text{for solid boundary nodes} \end{cases}
$$

where N is the number of particles that influence the pressure at the point $\vec{x}_i$, $\hat{p}_j$ are the nodal variables and $\Phi_j(\vec{x})$ is the shape function which is formulated by MLS method [27]. The particles movement will be based on the minimum pressure gradient, as detailed in Sriram and Ma [31].

2.4 Motion of floating body

The translational motion of the centre of gravity (CG) and rotational motion of the floating body is given in a simple 2D framework by

$$
m \frac{d\vec{V}_C}{dt} = \vec{F} + m\vec{g} \tag{17}
$$

$$
I_C \frac{d\dot{\theta}}{dt} = \vec{M} \tag{18}
$$

where m is the mass of the floating body, I_C is the mass moment of inertia about the CG of the floating body, $\vec{V}_C$ is the translational velocity of CG and $\dot{\theta}$ is the angular velocity of the floating body. $\vec{F}$ is the net hydrodynamic force and $\vec{M}$ is the net hydrodynamic moment acting on the floating body.

The floating body surface consists of a series of particles. Once the pressure acting on the floating body particles are evaluated by Eq.15 the hydrodynamic force and hydrodynamic moment acting on the floating body can be estimated by using the following equations:

$$
\vec{F} = \iint_{S_I} p_I \vec{n} ds \tag{19}
$$

$$
\vec{M} = \iint_{S_I} (\vec{r}_I - \vec{r}_C) \times p_I \vec{n} ds \tag{20}
$$

where $\vec{r}_I$ is the position vector of particle I on the surface of the floating body and $\vec{r}_C$ is the position vector of the CG of the floating body. The velocity of the particles on the free surface of the floating body is updated by using the equation of rigid body dynamics as given below:

$$
\vec{U}_I = \vec{V}_C + \dot{\theta} \times (\vec{r}_I - \vec{r}_C) \tag{21}
$$

The value of $\vec{U}^{n+1}$ while solving Eq. 15 is unknown. An iterative technique described by Yan and Ma [36] for fully nonlinear potential flow theory is being used in the present formulations. The algorithm is briefly described here:

i. Predict the accelerations of the floating body $\left(\frac{d\vec{V}_C}{dt} \text{ and } \frac{d\dot{\theta}}{dt}\right)$ at $(n+1)^{th}$ time step using Adams-Bashforth method:

$$\frac{d\vec{V}_C^{n+1}}{dt} = \left(\frac{3}{2}\frac{d\vec{V}_C^n}{dt} - \frac{1}{2}\frac{d\vec{V}_C^{n-1}}{dt}\right) \tag{22}$$

Replace $\vec{V}_C$ with $\dot{\theta}$ in Eq. 22 for getting $\frac{d\dot{\theta}^{n+1}}{dt}$.

ii. Estimate corresponding body velocities $\left(\vec{V}_C \text{ and } \dot{\theta}\right)$ at $(n+1)^{th}$ time step using Adams-Moulton method:

$$\vec{V}_C^{n+1} = \vec{V}_C^n + \frac{\Delta t}{12}\left(5\frac{d\vec{V}_C^{n+1}}{dt} + 8\frac{d\vec{V}_C^n}{dt} - \frac{d\vec{V}_C^{n-1}}{dt}\right) \tag{23}$$

Replace $\vec{V}_C$ with $\dot{\theta}$ in Eq. 23 for getting $\dot{\theta}^{n+1}$.

iii. Evaluate particle velocity $\vec{U}^{n+1}$ on the surface of the floating body using Eq.21 and substitute in Eq.15.

iv. Solve Eq. 16 and estimate the pressure.

v. Find out the net force $\vec{F}$ and net moment $\vec{M}$ acting on the floating body from Eq.19 and Eq.20.

vi. Calculate new accelerations $\left(\frac{d\vec{V}_C}{dt} \text{ and } \frac{d\dot{\theta}}{dt}\right)$ from Eq.17 and 18.

vii. Determine new body velocities $\left(\vec{V}_C \text{ and } \dot{\theta}\right)$ at $(n+1)^{th}$ time step from Eq.23 by replacing predicted $\frac{d\vec{V}_C}{dt}$ and $\frac{d\dot{\theta}}{dt}$ in step 'i' with $\frac{d\vec{U}_C}{dt}$ and $\frac{d\dot{\theta}}{dt}$ calculated in step 'vi'.

viii. Calculate new particle velocity $\vec{U}^{n+1}$ on the surface of the floating body from Eq.21 by using new body velocities.

ix. Repeat step 'iv' to 'viii' till the relative error in forces between two iterations is small enough.

x. Update the position of the CG for the floating body using the final velocities $\left(\vec{V}_C \text{ and } \dot{\theta}\right)$ and accelerations $\left(\frac{d\vec{V}_C}{dt} \text{ and } \frac{d\dot{\theta}}{dt}\right)$ obtained in the above loop (step 'iv' to 'viii') by using the third-order Taylor series expansion,

$$\vec{r}_C^{n+1} = \vec{r}_C^n + \vec{V}_C^{n+1}\Delta t + \frac{\Delta t^2}{2}\frac{d\vec{V}_C^{n+1}}{dt} + \frac{\Delta t^3}{6}\frac{d}{dt}\left(\frac{d\vec{V}_C^{n+1}}{dt}\right) \tag{24}$$

Replace $\vec{V}_C$ with $\dot{\theta}$ and $\vec{r}_C$ with θ in Eq. 24 in order to get the angular displacement θ^{n+1}.

The high-order equation for predicting the acceleration (Eq. 22) is used to decouple the mutual relation between the pressure boundary conditions on the floating body surface and the body acceleration. In other words, to solve the pressure, one needs to have body acceleration, which is unknown and need to be predicted. The high order scheme is just used to predict body acceleration, which will be corrected through the iteration. Theoretically, if the acceleration result is convergent, we can use any scheme for the prediction. In our tests done with the linear scheme the iterations, does not give convergent body acceleration, typically cannot ensure the numerical stability, that is why we used the high-order for the prediction. The integration of the floating body equations needs careful consideration for the overall stability and remove the error propagation into the domain over the period of time. Otherwise, one need to do some kind of high pass filtering to remove the noise near to the floating body. So, high-order schemes are applied to update the velocity (Eq. 23) and position (Eq. 24) and to get better convergence in one iteration per time step (see section 3.2.2).

2.5   Pressure gradient calculation

Once the fluid particle pressure is estimated, the gradient of pressure needs to be calculated to update fluid particle velocity in Eq.10. The IMLPG_R method uses SFDI scheme to evaluate the pressure gradient[29]. Since fluid particles are distributed only on one side of the boundary the pressure gradient calculation near the boundaries may not be correct. This will not be a major issue for the wave interaction with fixed structures, whereas it will make numerical issues for wave interaction with floating body problems because of the floating body boundary movement. So, this work considers ghost particles (imaginary particles) on the other side of the wall to compensate for the fluid particle deficiency. The position and pressure of these ghost particles are determined by using fixed ghost particle technique proposed by Marrone et al[37,38]. In this method, the ghost particles are fixed with respect to the reference frame of the body and are created along with the initial node generation. Each ghost particle is associated with an interpolation point inside the fluid domain and the position vector $\vec{r}^*$ of interpolation point is obtained by mirroring the position of the ghost particle $\vec{r}_s^*$ into the fluid domain. The ghost particle pressure p_s is determined by using the equation given below:

$$p_s = p^* + \frac{\partial p}{\partial n}.\left(\vec{r}^* - \vec{r}_s\right) \tag{25}$$

where p^* is the interpolation point pressure, which is calculated by interpolating the fluid pressure in the local sub-domain of the interpolation point, and

$$\frac{\partial p}{\partial n} = \rho\left[\vec{g}.n - \frac{D\vec{U}}{Dt}.n + \upsilon\nabla^2\vec{u}.n\right] \tag{26}$$

Eq. 26 is obtained from Eq. 2. The ghost particles are considered only for pressure gradient calculation. After estimating the pressure gradient, the velocity and position of fluid particles are updated by using Eqs. 10 and 11.

2.6   Free surface identification technique

The fluid particles discretizing the computational domain are classified into two groups: free surface particles and internal particles. If the wave is non-breaking or if the wave does not interact with structures, then the free surface at the beginning of the computation can be kept as the same for the entire simulation. For breaking waves and for wave-structure interaction problems the fluid particles initially on the free surface may submerge into the inner domain and fluid particles in the inner domain may rise on to the free surface. So, it is necessary to identify and update the free surface in each time step. Free surface identification is challenging, in particle methods especially in true mesh free methods like MLPG_R method which do not use global background mesh. In this work, the free surface is updating in a two-step procedure. First, the simple free surface identification technique proposed by Barecasco et al[39] is used to find out the particles which have more tendency to become the free surface. Next step will reconfirm whether the particle is really a free surface particle by using the procedure detailed in Ma and Zhou [30]. This two-step method will overcome the difficulties associated with particle number density (commonly used in MPS/ISPH, Koshizuka et al., [7]) which requires uniform particle distribution.

2.7 Variable spaced particle distribution

In order to capture the accurate flow characteristics of the wave-structure interaction problems, particularly in problems involving floating structures, very fine particle resolution needs near the structure. Wave-floating structure interaction problems also demand the fine particle distribution to predict the angular displacements (roll in the 2D problem) exactly. Usually, the fluid domain away from the structure requires only a low resolution compared to particle distribution near the structure. If uniform particle distribution with fine resolution is applied to discretize the fluid domain, total particle number becomes very high, and this issue increases the computation cost drastically for problems having a large domain. In this present work, in order to reduce the computation cost and increase the body response accuracy, total particle number is reduced by applying variable spaced particle distribution method, in which fine resolution of particles is given to fluid domain near the structure and coarse resolution is applied to domain far from the structure. In the previous work, single or twin body forced response [40], sudden change in the particle resolutions are carried out, as oscillations from body can be allowed to damp out after generations and no need to care about the outgoing waves for those applications. This is due to the fact that the sudden change in the particle leads to the unequal node spacing on either side of the support domain as shown in Fig. 1a. If one uses support domain size from smaller nodes leads to gap on the left side (Fig. 1b) and vice versa (Fig. 1c). Further, this method may also lead to identification of the free surface particle inside the domain, which will be major issue. Moreover, for wave-floating body interactions, this method of generations failed to resolve the incoming waves. Hence, different approach is carried out. Fig. 1d shows the model of variable spaced particle distribution used in this work to discretize the fluid domain. The particle spacing near the structure should be small enough to obtain motion of the floating body and the particle spacing outside the domain is based on the minimum number of particles required for capturing the wave elevation. In Fig. 1d the particle distribution near the structure and far field are uniform. In the space between this far field and near field, there is an intermediate field, where the particle spacing gradually decreasing from maximum spacing in the far field to minimum spacing in the near field like in conventional finite element method. The ratio of the particle spacing γ in two adjacent layers (if moving from far field to near field) should be optimum for best results.

Let n be the number of layers in the intermediate field and Δx_0, Δx_1, Δx_2……… Δx_n are the particle spacing in each layer if moving from the outer coarse spaced layer to inner fine spaced layer. Δx_0 be the initial particle spacing in the outer uniformly spaced region and Δx_n be the initial particle spacing in the inner uniformly spaced region. The particle spacing in the variable spaced intermediate region can be obtained by

$$\Delta x_i = \gamma \Delta x_{i-1} \qquad\qquad\qquad (27)$$

where i represents the layer number and γ is the ratio of the particle spacing from finer to coarser. Δx_{n-1} should be less than or equal to Δx_n.

In order to handle the variable particle spacing, in the IMLPG_R method, the radius of the support domain for each particle interactions are considered as dynamic and is modified to:

$$R(I) = \frac{R(I) + R(J)}{2} \qquad\qquad (28)$$

where *I* is the particle under consideration and *J* is the neighbouring particle.

3 NUMERICAL TESTS AND DISCUSSION

3.1 Roll decay test

The major challenge in 2D wave-floating structure interaction problem is the exact prediction of the roll motion of the floating body. Accurate prediction of roll motion demands very fine spacing near the structure. In order to find out the optimum particle spacing and to validate the proposed numerical method simulation for free roll decay, a rectangular floating body in calm water is considered. The experimental data of Ren et al [21] is used for this test. They performed damped roll oscillation of a rectangular floating body having dimensions 0.3m×0.2m in a wave flume. The water depth of the flume is 0.4m and draft of the body is 0.1m. The initial roll displacement θ_0 given to the body is 11.5^0 (The roll angle is measuring with respect to the vertical axis and the inclination is positive in the clockwise direction and negative in the counter-clockwise direction). The same test has been simulated in a numerical wave tank (NWT) with water depth of 0.4m and tank length of 3m. The centroid of the floating body is fixed at point (1.5,0.4). Uniform particle distribution is considered in this test as the variable particle spacing is not of much importance for this study.

The roll decay test for different spatial resolutions (Δx) and time step sizes (Δt) are performed and the time histories of roll angle are compared in Fig. 2 and Fig. 3. The value of Δt is calculated with respect to the roll decay period T_r. The experimental value of roll decay period for the floating body considered is 1.6s. $\Delta t = T_r/150$, $T_r/200$, $T_r/250$ and $T_r/300$ are considered for the test. The test showed that the time step size of Δt=0.008s ($T_r/200$) is the maximum time step size that can use for the simulation. Further increase in time step size ($T_r/150$) causes large fluid particle displacement near the corners of the floating body and stops the simulation suddenly. So, the convergence test for space is performed with time step size Δt=0.008s. In Fig. 2, the time histories obtained with Δx=0.005m and Δx=0.004m are found to be very close. So, Δx=0.005m can be accepted as the optimum particle spacing. Then, the convergence test for time is done with Δx=0.005m. Fig. 3 presents the comparison of time histories of roll angle for different time step size and it can be seen that Δt=0.0064s is the optimum time step value for the simulation and more reduction in time step size damp-out the amplitude of roll after two or three cycles of oscillation. So Δx=0.005m with Δt=0.0064s is the best particle spacing and time step size respectively for the roll decay test. Further, the time history of roll motion obtained with Δx=0.005m and Δt=0.0064s is compared with experimental as well as WCSPH results of Ren et al[21] and ISPH_BS result of Zheng et al[24]. The comparison is shown in Fig. 4 and the IMLPG_R result shows good agreement with the experimental result.

3.2 Wave interaction with the freely floating body

3.2.1 With uniform particle distribution

In this section, the motion of a freely floating body under regular waves is considered initially with uniform spacing. The waves are generated in a numerical wave tank (NWT). The NWT has piston type paddle on the left side to generate waves and damping zone on the right side to avoid wave reflection from tank wall. The water depth and tank length of the NWT are 0.4m and 20m respectively. The coordinate system O-xy is fixed at the bottom left corner of the NWT with x positive in rightward direction and y positive in upward direction. The same floating body used for free roll decay test is used for this test. The schematic diagram for wave interaction with the freely floating body is shown in Fig. 5. The initial position of the centroid of the floating body is at the point (5.15, 0.4). The floating body is free to sway, heave and roll. The centroid of the floating body is used to track the motion of the floating body in sway as well as heave direction and the inclination of the initial vertical axis of the rectangular floating box with y-axis is used to measure the roll motion of the floating body. The wave paddle motion is sinusoidal and propagating in x-direction. The simulations are carried out with two different waves, one is linear wave (H=0.04m, T=1.2s) and second is strong nonlinear wave (H=0.1m, T=1.2s). The NWT is discretized uniformly in both directions.

As a first step, convergence study for space and time is performed to understand the efficiency for wave interaction with floating body problems. The wave characteristics used for the convergence test is H=0.04m and T=1.2s. Similar to roll decay test the maximum time step size that can be used for the simulation is T/200. Larger time step size breaks the simulation because of the fast particle displacement near the floating structure. Hence, the convergence test for space has been conducted for time step size Δt=0.0048s (T/250). The particle spacing considered are Δx=0.01m, 0.00625m, 0.005m and 0.004m. The comparison of time histories of motion trajectories obtained with different particle spacing when Δt=0.0048s is shown in Fig. 6. It can be seen that sway and heave motion of the floating body is matching in all Δx, whereas the roll response of the body shows a very close match for Δx=0.005m and Δx=0.004m only. Considering the motion of the body in three degrees of freedom, Δx=0.005m will be the optimum spacing for simulation. Then, the convergence test for time step size is conducted with Δx=0.005m and the results are compared in Fig. 7. The figure clearly indicates that Δt=0.0048s is the optimum value of time step size. So Δx=0.005m and Δt=0.0048s is used as the particle spacing and time step size respectively for further simulations.

The optimum values of Δx and Δt are now compared with the time history of the free surface elevation from experimental as well as numerical (WCSPH method) results of Ren et al[21]. This is shown in Fig. 8. The wave elevation generated from IMLPG_R method shows satisfactory agreement with literature results. Similarly, the comparison of time histories for motion characteristics of the freely-floating box under regular waves with experimental as well as WCSPH result of Ren et al[21] and ISPH_BS result of Zheng et al[24] for small and steep waves are given in Fig. 9 & Fig. 10. In these figures, the heave and roll components of motion show simple harmonic oscillations because of stability of body in heave and roll direction, whereas the sway

component of motion shows simple harmonic oscillations with a drift motion in the wave propagating direction (*x*-direction). The drift motion is due to mean drift force generated by wave propagation. Further, the spatial motion of the centroid of the floating body in small amplitude wave and steep wave is compared with the experimental and numerical result of Ren et al[21] in Fig. 11. This comparison also shows good agreement with experimental results. Since all the results are matching very well with the experimental results, the IMLPG_R method is found to be robust for simulating wave-floating body interaction problems.

3.2.2   With variable spaced particle distribution

The primary aim of the present work is to adopt variable spacing approach, so that one can decrease the total number of particles at the far end, since the $\Delta x/\Delta t$ ratio used for above simulations are 1.041667m/s, whereas using IMLPG_R for modelling wave propagations or rigid structure $\Delta x/\Delta t$ ratio greater than 4m/s is sufficient Sriram and Ma[31]. This fine resolution is mostly required to capture the roll motions properly, even for potential based method (see Yan and Ma[36], it requires minimum 200 nodes near the body). Thus, one requires variable particle spacing. In this section, variable spaced particle distribution discussed in section 2.7 is studied. The results obtained with variable spaced particle distribution and uniform particle distribution will compare only if there is no damping of the wave between two adjacent layers of particles. Taking this considerations, numerical tests are carried out. Hence, the value of γ in Eq.27 is very important to avoid damping of flow characteristics. Small value of γ means, number of layer of particles in the intermediate region is small. As the value of γ increase, the number of layer of particles in the intermediate region will increase. Also, the width of intermediate region will become big with respect to γ, because the variation of particle spacing from coarse region to fine region will be slow. Assume, the width of fine spaced region (near field) is constant, then the width of coarse spaced region (far field) will decrease with respect to value of γ. All these will increase total number of particles. So, in order to obtain the optimum value of γ, the simulation done in section 3.2.1 are re-simulated with variable spaced particle distribution for different values of γ varying from 0.5 to 0.9. The time history of free surface elevation obtained at different positions (*x*=2m (wave probe-1), *x*=4m (wave probe-2) and *x*=4.9m (wave probe-3) from the wave maker as shown in Fig. 12 (with uniform particle distribution) is compared with the variably spaced particle distribution for *H*=0.04m and *T*=1.2s. Δx_0=0.02m (nearly 100 particles per wavelength) and Δx_n=0.005m is used. Thus, $\Delta x/\Delta t$ is 1m/s near the floating body and 4m/s elsewhere in the domain. Fig. 13 compares the time histories of wave elevation obtained from the wave probe at different positions. It can be seen that when γ=0.5, the free surface elevation obtained at 2m from wave maker have small damping after five periods of wave, the wave probe recording at 4m from wave maker have large noises and wave probe-3 has small irregularities compared to results obtained with uniform particle distribution. This can be explained with the fact that value of γ causes insufficient number of particles in the supporting domain of each particle inside the intermediate region. The lack of an ample number of particles inside the support domain results in the incorrect estimation of flow characteristics. So, the incoming wave propagation from far field to near field and reflected wave propagation from the floating body to far-field does not cross the intermediate region smoothly. Hence, the time history of the free surface has sudden peaks.

Fig. 13 also shows the wave elevation results obtained from variable spaced particle distribution with γ=0.6&0.9 and these are in agreement with uniform particle distribution results. The value of γ=0.9 leads to larger number of nodes in the intermediate regions, which in fact is not required. So, γ=0.6 can be considered as the optimum value for accurate prediction of flow characteristics as it requires a smaller number of particles compared to γ=0.9. The reliability of γ=0.6 is checked by performing the above simulation for steep wave case (H=0.1m and T=1.2s). The wave probe data obtained are compared with uniform particle distribution in Fig. 14. This figure clearly indicates that γ=0.6 can be accepted as the optimum value. The time histories of sway, heave and roll motion of the floating body for small and steep wave, with variable spacing and uniform spacing are compared in Fig. 15 & Fig. 16. Also, the spatial movement of the centroid for these cases is also compared in Fig. 17. All these results prove that IMLPG_R method with variable spaced particle distribution can replace the uniform particle distribution.

One of the important considerations during performing the wave interaction with a freely floating body problem using variable spaced particle distribution is the length of the near field uniformly spaced domain. Since, the floating body is free to move in the fluid domain, make sure that the floating body is always inside the fine spaced region. For this, initially, the length of the fine spaced region near or right side of the body should be large enough during the entire simulation period to capture the motion accurately. The length of the fine spaced region near the structure is small for small wave and long for steep wave, due to the large drift motion of the floating body in steep wave (Fig. 11). This is mainly due to the resolved spacing near the floating body.

Table 1 shows the comparison of computational time taken to simulate the wave interaction with floating body problem using variable and uniform particle distribution. It clearly shows that the variable spaced particle distribution requires only about 10% of the computational time used by the uniform particle distribution for the above problem. The computations are carried out in Intel core i7 with 32 GB RAM (Parallel mode for GMRES solver – 4 cores).

All the above tests performed are with only one iteration in the algorithm described in section 2.4 (step ix), i.e. the accelerations predicted in step i of section 2.4 are corrected only once (step vi) in each time step and the acceleration correction till convergence (step ix) is not carried out. Fig. 18 to Fig. 21 compared the time histories of different motion characteristics with different types of iterations for small as well as steep wave. It can be seen that the iteration till convergence does not have any effect on the result. Further,

Table 2 compares the time consumed for the above simulations and it can be found out that the iteration till convergence increases only the computation time and does not have any role in improving the result. So IMLPG_R method with variable spaced particle distribution with single iteration in each time step is enough for getting a good result for wave interaction with floating body problems. This is mainly achieved by using high order time schemes to solve floating body motion (Eq. 22~24) and resolved spacing near the floating body.

For interpretation, the position of the floating body at different instants of time in a wave period (t_0 is the initial time at which the floating body is horizontal) for H=0.04m and H=0.1m is shown in Fig. 22. The IMLPG_R method clearly captured the movement of the floating body in wave.

Compared to small wave (*H*=0.04m), in steep wave interaction, the floating body returns to its horizontal position at t_0 +1.09T. This is due to the large drift motion of the floating body in steep waves. Because of this large drift motion, the wave period experienced by the floating body differs from the actual wave period. Hence, there is a lag in floating body motion.

3.3 Green water impact load on the floating structure

To check the robustness of the proposed model, green water impact loading of the floating body is performed. The experimental results from Zheng et al [24] is used for the validation of the test results. The schematic view of the problem including body dimensions are shown in Fig. 23. The initial draft of the body is 0.25m and water depth is 0.7m. The centre of gravity of the body is located at 0.13171m from the bottom of the body and the moment of inertia is 4.5717kgm². In order to measure the impact pressure, two pressure sensors are installed, one at water line position and another at the inner deck as shown in Fig. 23. The simulation is carried out for *H*=0.1m and *T*=1.2s and the impact pressure is compared with the experimental as well as ISPH_BS result of Zheng et al [24]. The $\Delta x/\Delta t$ ratio used for the simulation is 1.25m/s near the floating body and 4m/s elsewhere in the domain. The comparison of impact pressure is shown in Fig. 24. It can be seen that the IMLPG_R result shows good agreement with experimental results as well as ISPH_BS results. The small deviations in the results may be due to the air-entrapment in the experiments and the present model is based on single phase flow. The spikes in the pressure time history might be due to the numerical interaction between incoming waves and fluid flow from the deck. This may result large fluid particle displacement near the free surface near to floating body. This large particle displacement leads to some misidentification of the free surface particle, leading to pressure oscillations. However, the same pressure fluctuations can also be seen in the experimental result also. The snapshot of the floating body movement at different instants of time is shown in Fig. 25, showing the splash up of the waves on the body and re-entering of the fluid into the domain.

4 CONCLUSION

In this paper, the variable spacing in the particle method has been implemented. The proposed method is simple and can be used in any meshless methods. The potential of this extension is of great importance in the sense that the application of the particle for floating body is feasible with a smaller number of particles, which is not possible otherwise. Further, the predictor-corrector scheme was implemented for the wave-floating-body interactions. It was shown that using the initial prediction with 2nd order Adam Bashforth method for acceleration and 3rd order Adams-Moulton method for velocities needs only single iterations instead of iterations till convergence, reducing further the time step (Δt=0.0048s is used for IMLPG_R method, whereas WCSPH method [24] used Δt=0.001s). To study the robustness and efficiency of the present IMLPG_R method, the simulations are performed with variable and uniform spaced particle distribution for small and steep waves. The variable spacing approach has a limitation leading to unequal nodal distribution for support domain, thus the tests are carried out to find the optimum value of γ. The optimum value of 0.6 shows good agreement between uniform and variable spaced particle distribution and reduced the computation time by 90% with respect to uniform particle distribution.

Finally, the robustness of the IMLPG_R method is tested by applying the model for green water impact loading of the floating structures and the results are validated with experimental data. Hence, the present IMLPG_R method with variable spaced particle distribution is a computationally efficient and reliable method for simulating steep wave interaction with floating body problems and can be easily extendable to 3D wave-floating body problems.

5   ACKNOWLEDGEMENT

6   References

[1]   B. Nayroles, G. Touzot, P. Villon, Generalizing the finite element method: Diffuse approximation and diffuse elements, Comput. Mech. 10 (1992) 307–318. doi:10.1007/BF00364252.

[2]   T. Belytschko, Y.Y. Lu, L. Gu, Element free Galerkin methods, Int. J. Numer. Methods Eng. 37 (1994) 229–256.

[3]   J.J. Monaghan, Simulating Free Surface Flows with SPH, J. Comput. Phys. 110 (1994) 399–406.

[4]   W.. Liu, Y. Chen, S. Jun, J.. Chen, T. Belytschko, C. Pan, R.. Uras, C.. Chang, Overview and applications of the reproducing Kernel Particle methods, Arch. Comput. Methods Eng. 3 (1996) 3–80.

[5]   S. Koshizuka, Y. Oka, Moving-particle semi-implicit method for fragmentation of incompressible fluid, Nucl. Sci. Eng. 123 (1996) 421–434.

[6]   H. Gotoh, A. Khayyer, On the state-of-the-art of particle methods for coastal and ocean engineering, Coast. Eng. J. 00 (2018) 1–25. doi:10.1080/21664250.2018.1436243.

[7]   S. Koshizuka, A. Nobe, Y. Oka, Numerical analysis of breaking waves using the moving particle semi-implicit method, Int. J. Numer. Methods Fluids. 26 (1998) 751–769. doi:10.1002/(SICI)1097-0363(19980415)26:7<751::AID-FLD671>3.0.CO;2-C.

[8]   M. Sueyoshi, Numerical Simulation of Extreme Motions of a Floating Body by MPS Method, in: Ocean. MTTS/IEEE TECHNO-OCEAN'04, IEEE, 2004: pp. 566–572. doi:10.1109/OCEANS.2004.1402977.

[9]   M. Sueyoshi, M. Kashiwagi, S. Naito, Numerical simulation of wave-induced nonlinear motions of a two-dimensional floating body by the moving particle semi-implicit method, J. Mar. Sci. Technol. 13 (2008) 85–94. doi:10.1007/s00773-007-0260-y.

[10]   H. Ikari, H. Gotoh, Abbas Khayyer, Numerical simulation on moored floating body in wave by improved mps method, in: Coast. Struct., 2011: pp. 308–317.

[11]   B. Lee, S. Jeong, S. Hwang, J. Park, M. Kim, A Particle Simulation of 2-D Vessel Motions Interacting with Liquid-Sloshing Cargo, C. Comput. Model. Eng. Sci. 91 (2013) 43–63.

[12] Y.L. Zhang, Z.Y. Tang, D.C. Wan, Numerical Study of Interaction between Waves and Floating Body by MPS Method, in: ICCM, 2015.

[13] J.J. Monaghan, A. Kos, Scott Russell 's wave generator, Phys. FLUIDS. 12 (2000) 622–630. doi:10.1063/1.870269.

[14] J.J. Monaghan, a Kos, N. Issa, Fluid Motion Generated by Impact, J. Waterw. Port, Coastal, Ocean Eng. 129 (2003) 250–259. doi:10.1061/(ASCE)0733-950X(2003)129:6(250).

[15] M. Doring, G. Oger, B. Alessandrini, P. Ferrant, SPH simulation of Floating Bodies in Waves, in: ASME 2004 23rd Int. Conf. Offshore Mech. Arct. Eng., American Society of Mechanical Engineers, 2004: pp. 741–747.

[16] G. Oger, M. Doring, B. Alessandrini, P. Ferrant, Two-dimensional SPH simulations of wedge water entries, in: ASME 2012 31st Int. Conf. Ocean. Offshore Arct. Eng. Am. Soc. Mech. Eng., 2012: pp. 803–822. doi:10.1016/j.jcp.2005.09.004.

[17] C. Ulrich, T. Rung, MULTI-PHYSICS SPH SIMULATIONS OF LAUNCHING PROBLEMS AND FLOATING BODY INTERACTIONS, in: ASME 2012 31st Int. Conf. Ocean. Offshore Arct. Eng., American Society of Mechanical Engineers, 2012: pp. 685–694.

[18] M.R. Hashemi, R. Fatehi, M.T. Manzari, A modified SPH method for simulating motion of rigid bodies in Newtonian fluid flows, Int. J. Non. Linear. Mech. 47 (2012) 626–638. doi:10.1016/j.ijnonlinmec.2011.10.007.

[19] R.B. Canelas, J.M. Domínguez, A.J.C. Crespo, M. Gómez-gesteira, R.M.L. Ferreira, A Smooth Particle Hydrodynamics discretization for the modelling of free surface flows and rigid body dynamics, Int. J. Numer. METHODS FLUIDS. 78 (2015) 581–593. doi:10.1002/fld.

[20] B. Bouscasse, A. Colagrossi, S. Marrone, M. Antuono, Nonlinear water wave interaction with floating bodies in SPH, J. Fluids Struct. 42 (2013) 112–129.

[21] B. Ren, M. He, P. Dong, H. Wen, Nonlinear simulations of wave-induced motions of a freely floating body using WCSPH method, Appl. Ocean Res. 50 (2015) 1–12. doi:10.1016/j.apor.2014.12.003.

[22] P. Omidvar, P.K. Stansby, B.D. Rogers, Wave body interaction in 2D using smoothed particle hydrodynamics (SPH)with variable particle mass, Int. J. Numer. Methods Fluids. 68 (2012) 686–705. doi:10.1002/fld.

[23] P. Omidvar, P.K. Stansby, B.D. Rogers, SPH for 3D floating bodies using variable mass particle distribution, Int. J. Numer. Methods Fluids. (2013) 427–452. doi:10.1002/fld.

[24] X. Zheng, X. Lv, Q.W. Ma, W. Duan, A. Khayyer, S. Shao, An improved solid boundary treatment for wave-float interactions using ISPH method, Int. J. Nav. Archit. Ocean Eng. 10 (2018) 329–347. doi:10.1016/j.ijnaoe.2017.08.001.

[25] S.N. Atluri, T. Zhu, A new Meshless Local Petrov-Galerkin (MLPG) approach in computational mechanics, Comput. Mech. 22 (1998) 117–127. doi:10.1007/s004660050346.

[26] H. Lin, S.N. Atluri, The Meshless Local Petrov-Galerkin (MLPG) method for solving incompressible Navier-Stokes equations, C. - Comput. Model. Eng. Sci. 2 (2001) 117–142. doi:10.1038/466815b.

[27] Q.W. Ma, Meshless local Petrov-Galerkin method for two-dimensional nonlinear water wave problems, J. Comput. Phys. 205 (2005) 611–625. doi:10.1016/j.jcp.2004.11.010.

[28] Q.W. Ma, MLPG method based on Rankine source solution for simulating nonlinear water waves, C. - Comput. Model. Eng. Sci. 9 (2005) 193–209.

[29] Q.W. Ma, A New Meshless Interpolation Scheme for MLPG_R Method, C. Model. Eng. Sci. 23 (2008) 75–90. doi:10.1016/j.cpr.2010.02.004.

[30] Q.W. Ma, J.T. Zhou, MLPG_R Method for Numerical Simulation of 2D BreakingWaves, C. - Comput. Model. Eng. Sci. 43 (2009) 277–303.

[31] V. Sriram, Q.W. Ma, Improved MLPG_R method for simulating 2D interaction between violent waves and elastic structures, J. Comput. Phys. 231 (2012) 7650–7670. doi:10.1016/j.jcp.2012.07.003.

[32] R. Divya, V. Sriram, Wave-porous structure interaction modelling using Improved Meshless Local Petrov Galerkin method, Appl. Ocean Res. 67 (2017) 291–305. doi:10.1016/j.apor.2017.07.017.

[33] A.S. Rijas, V. Sriram, Numerical simulation of floating body under heave oscillations using 2D IMLPG_R, Proc. Twenty Seventh Int. Ocean Polar Eng. Conf. (2017) 630–636.

[34] A.S. Rijas, V. Sriram, S. Yan, Numerical Simulation of 2D Wave-Structure Interaction Using IMLPG_R, in: Proc. Twenty Eighth Int. Ocean Polar Eng. Conf., International Society of Offshore and Polar Engineers (ISOPE), 2018: pp. 264–271.

[35] A.J. Chorin, Numerical Solution of the Navier-Stokes Equations, Math. Comput. 22 (1968) 745–762. doi:https://doi.org/10.1090/S0025-5718-1968-0242392-2.

[36] S. Yan, Q.W. Ma, Numerical simulation of fully nonlinear interaction between steep waves and 2D floating bodies using the QALE-FEM method, J. Comput. Phys. 221 (2007) 666–692. doi:10.1016/j.jcp.2006.06.046.

[37] S. Marrone, M. Antuono, A. Colagrossi, G. Colicchio, D. Le Touzé, G. Graziani, δ-SPH model for simulating violent impact flows, Comput. Methods Appl. Mech. Eng. 200 (2011) 1526–1542. doi:10.1016/j.cma.2010.12.016.

[38] S. Marrone, A. Colagrossi, M. Antuono, C. Lugni, M.P. Tulin, A 2D+t SPH model to study the breaking wave pattern generated by fast ships, J. Fluids Struct. 27 (2011) 1199–1215. doi:10.1016/j.jfluidstructs.2011.08.003.

[39] A. Barecasco, H. Terissa, C.F. Naa, Simple free-surface detection in two and three-dimensional SPH solver, ArXiv Prepr. ArXiv1309.4290. (2013). http://arxiv.org/abs/1309.4290.

[40] A.S. Rijas, V. Sriram, Numerical modelling of forced heaving of mono hull and twin hull in particle method, Ocean Eng. 173 (2019) 197–214. doi:10.1016/j.oceaneng.2018.12.066.

Floating body

(a)

(b)

(c)

(d)
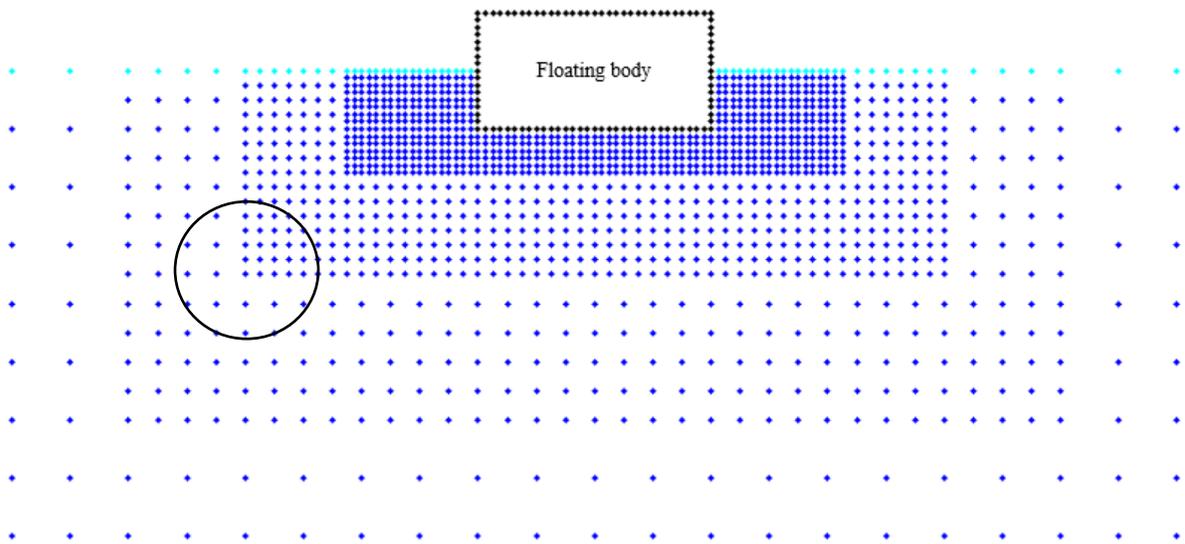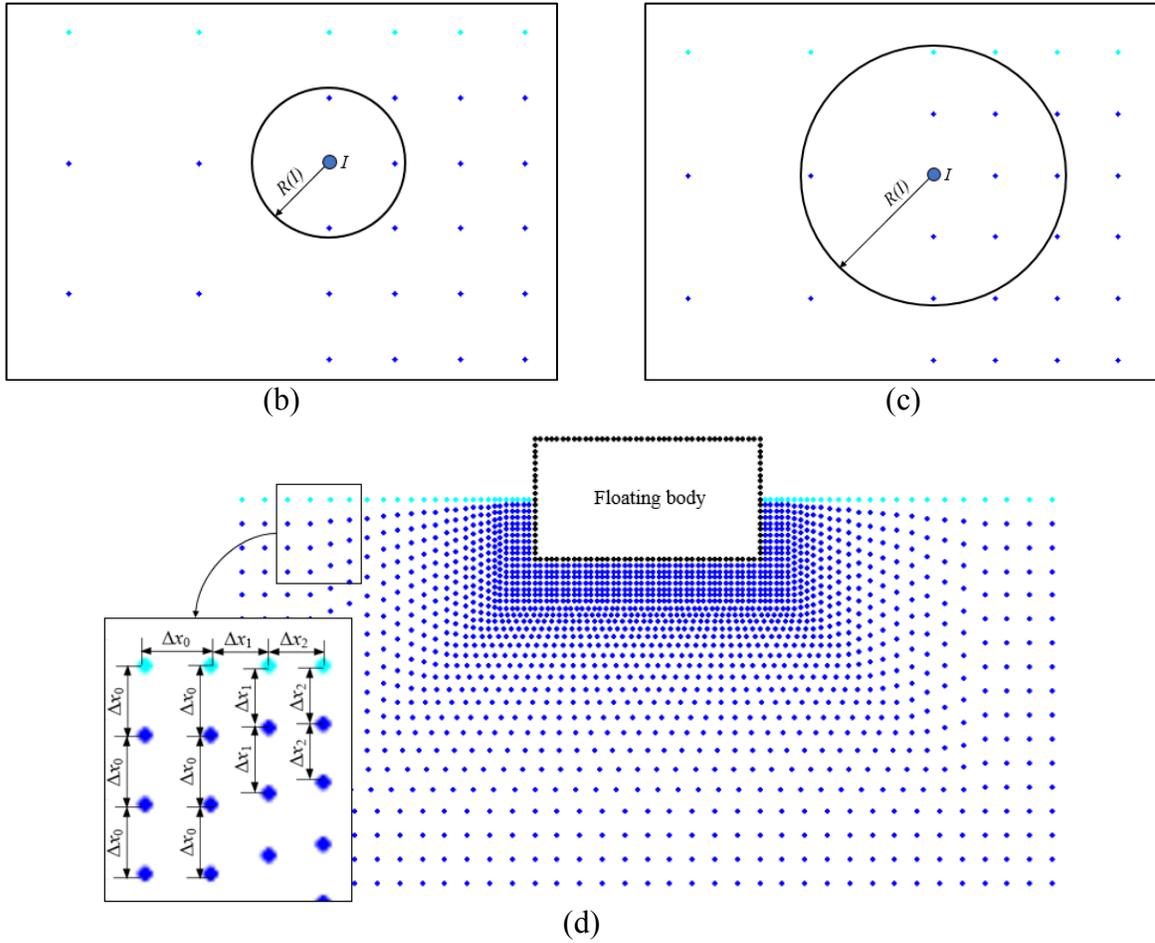
Fig. 1. Variable spaced particle distribution.
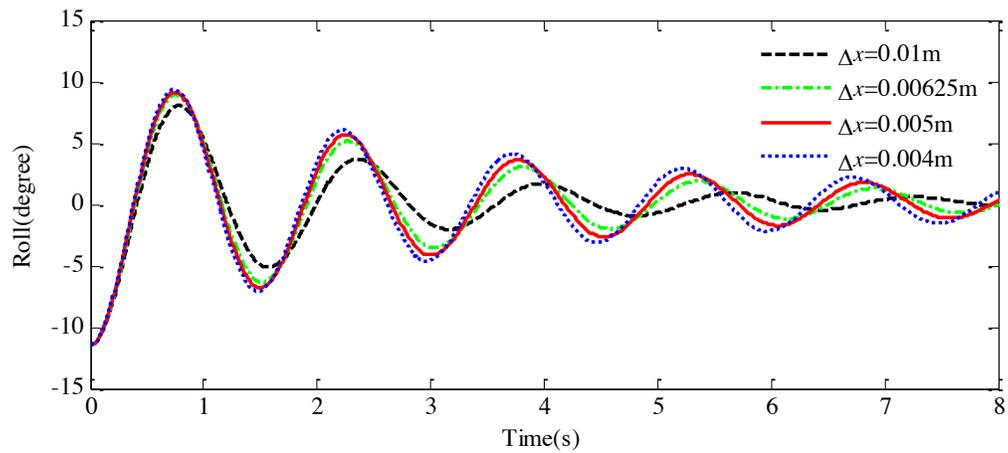
Fig. 2. Comparison of time histories of roll angle for different particle spacing when Δt=0.008s.
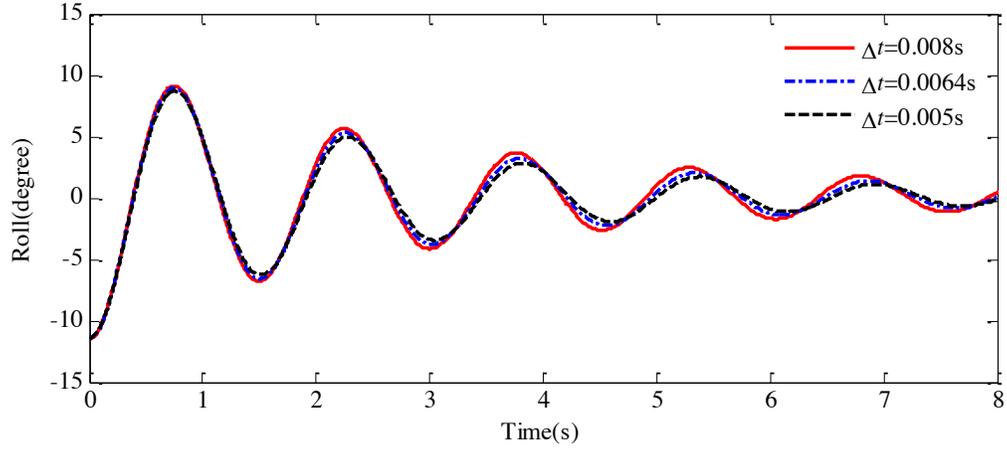
Fig. 3. Comparison of time histories of roll angle for different time step sizes when particle spacing Δ*x*=0.005m.
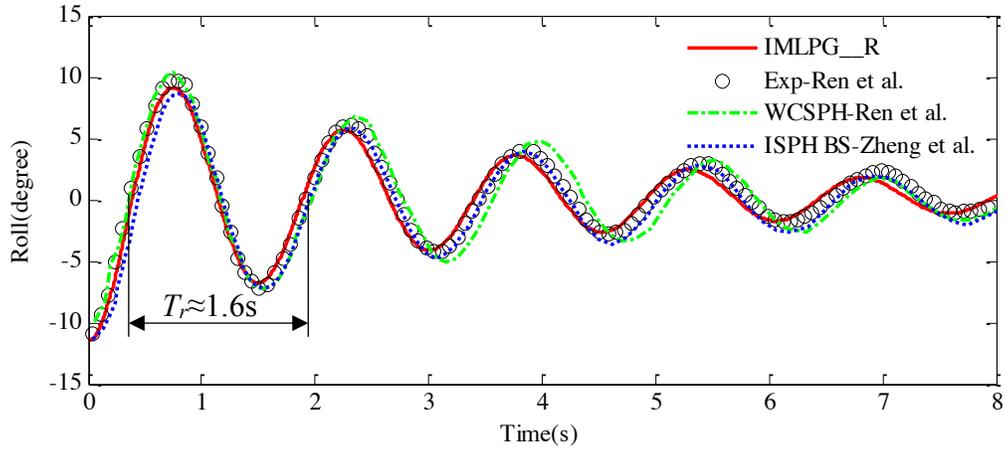
Fig. 4. Comparison of time histories of roll angle with (a) experimental and WCSPH result of Ren et al[21] (b)ISPH BS result of Zheng et al[24].
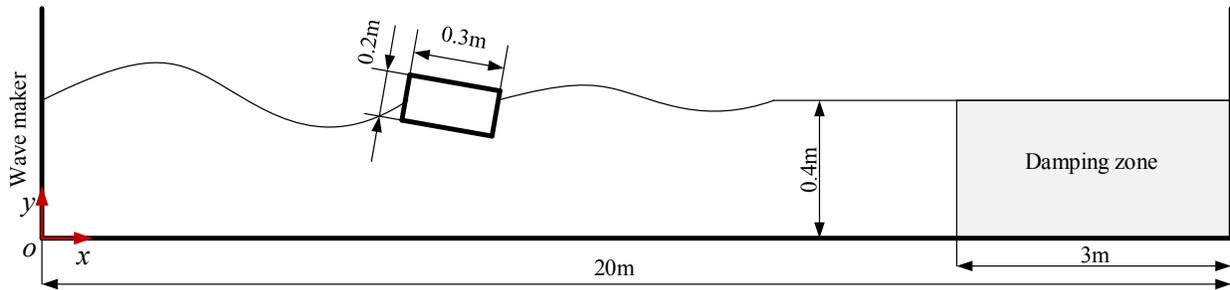
Fig. 5. Schematic diagram for wave interaction with a floating body.
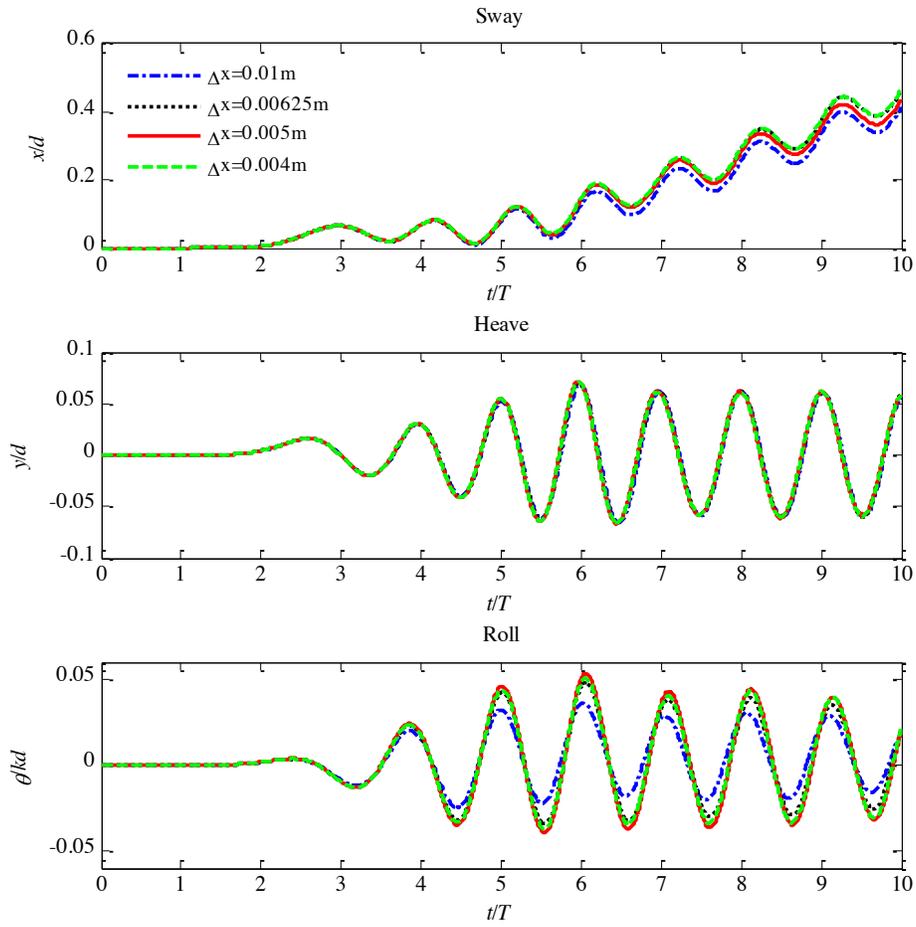
Fig. 6. Comparison of time histories of motion trajectories for different particle spacing when Δ*t*=0.0048s.
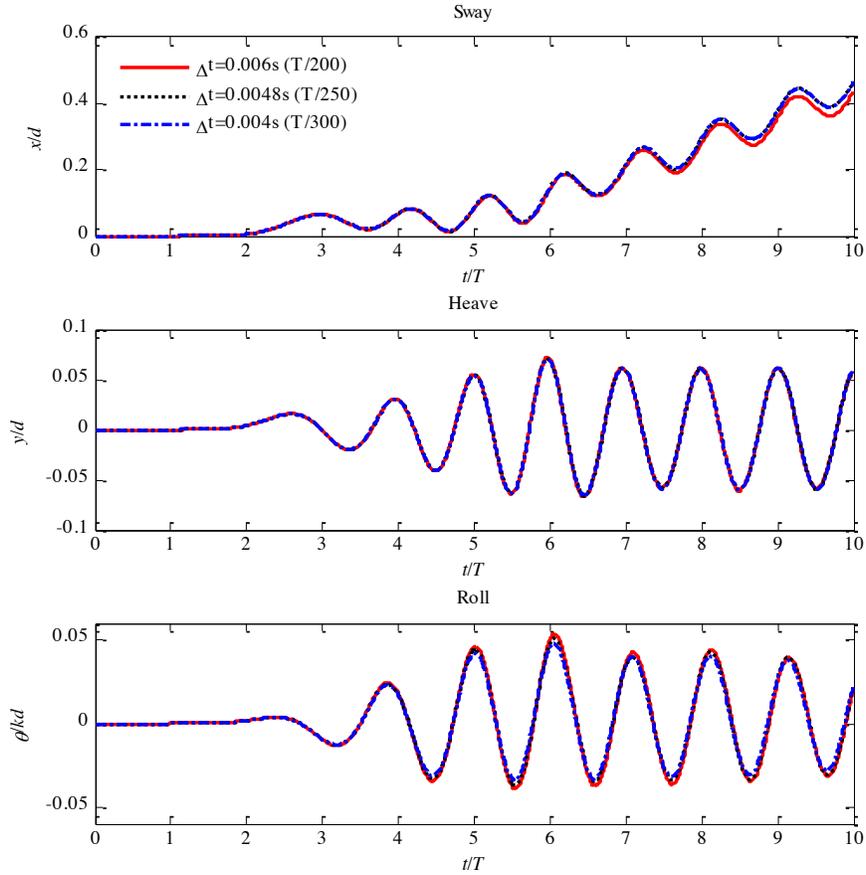
Fig. 7. Comparison of time histories of motion characteristics for different time step sizes when particle spacing Δx=0.005m.
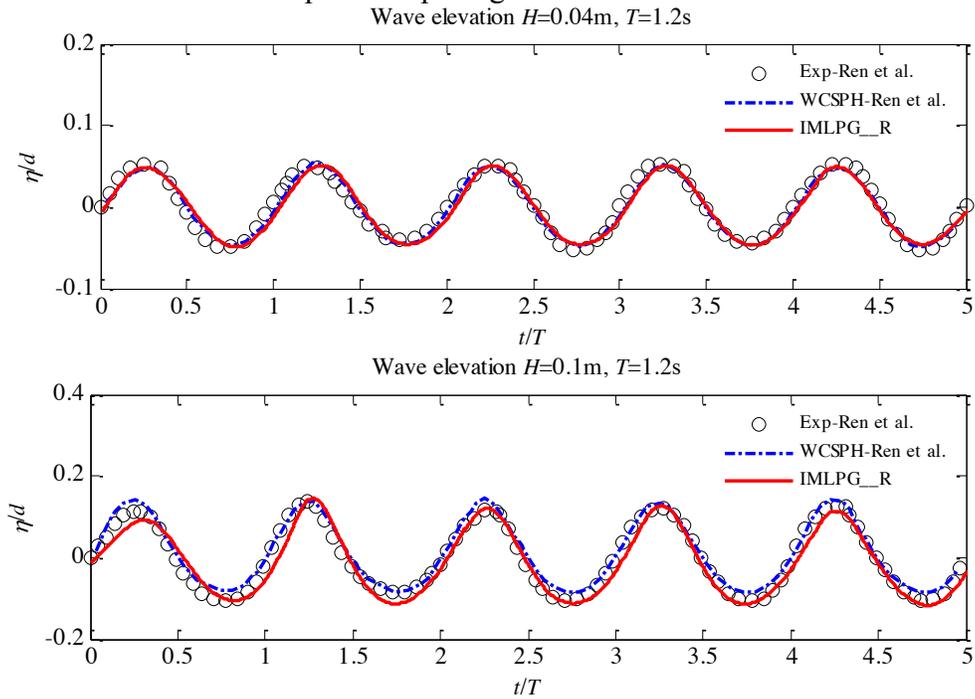
Fig. 8. Comparison of time histories of free surface elevation.
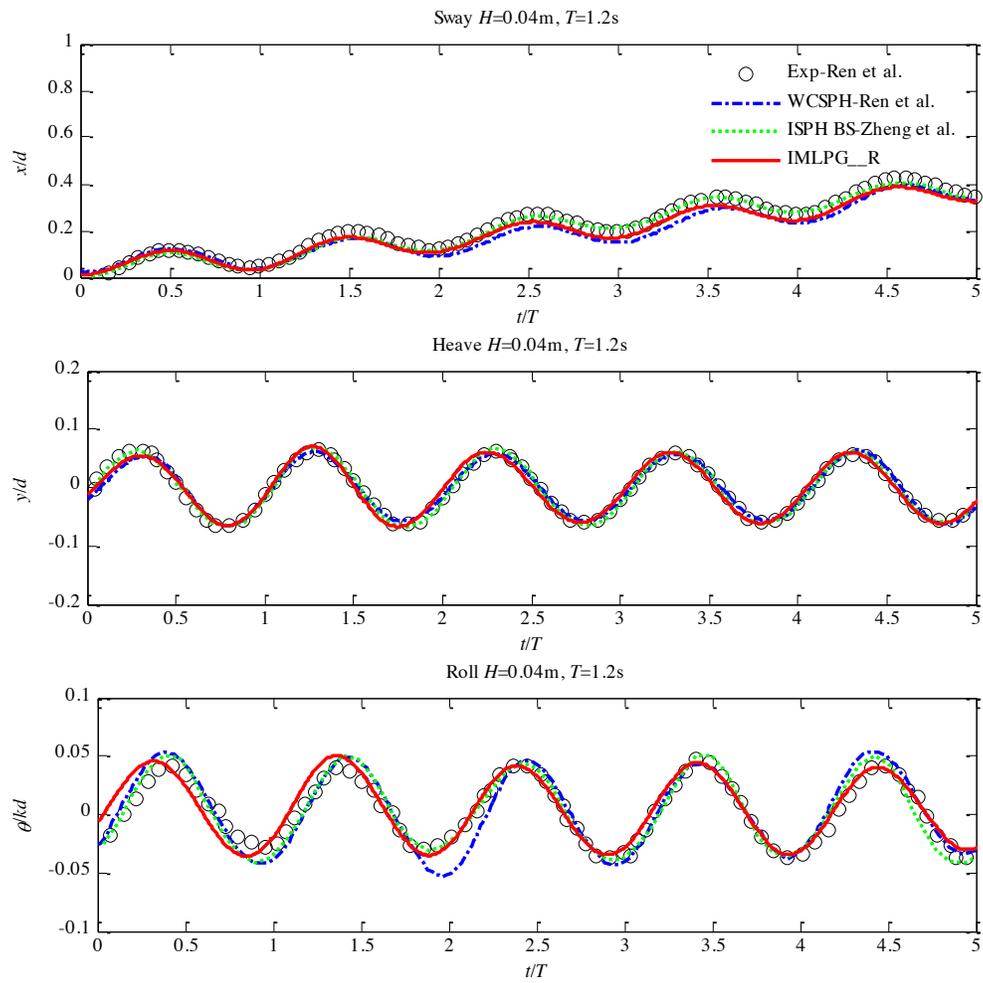
Fig. 9. Time histories of the motion characteristics of the free-floating box under the regular wave with H=0.04m and T=1.2s.
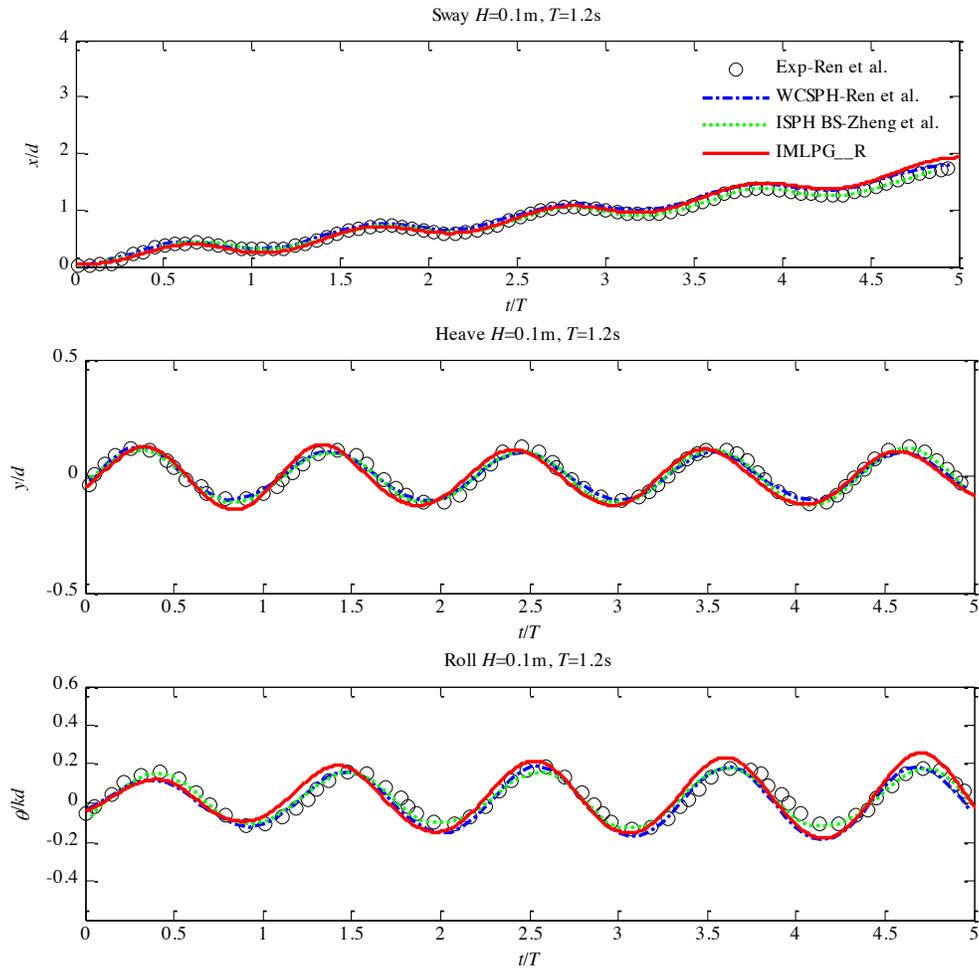
Fig. 10. Time histories of the motion characteristics of the free-floating box under the regular wave with H=0.1m and T=1.2s.
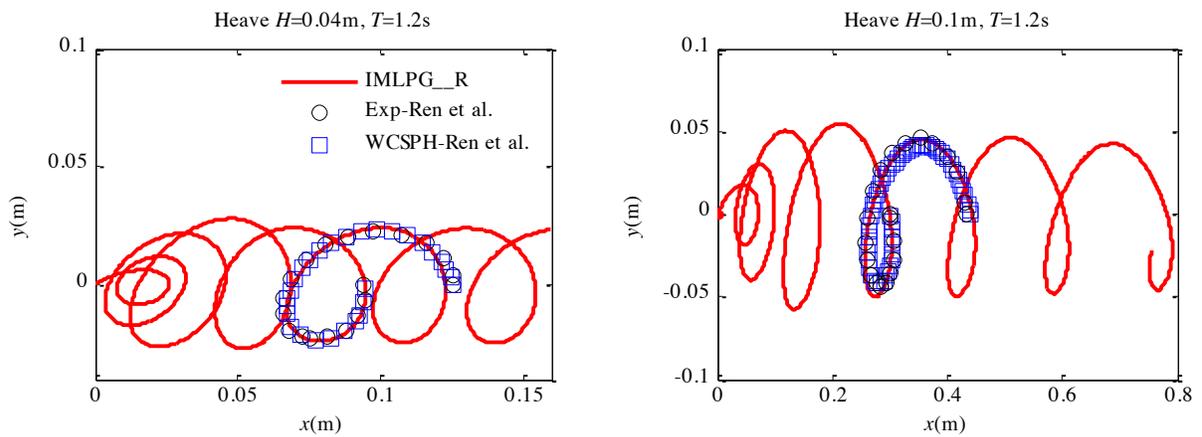
Fig. 11. The trajectory of the centroid of the floating box in motion.
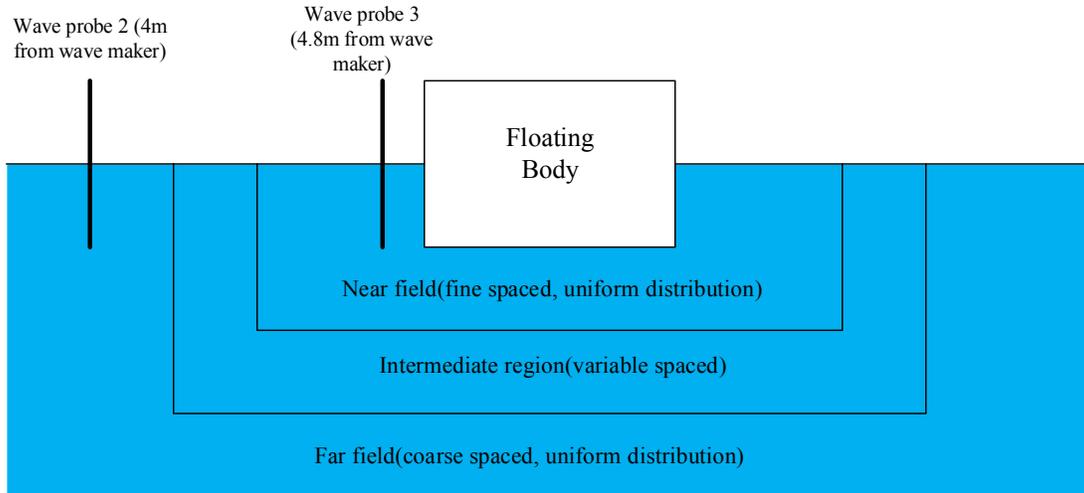
Fig. 12.Schematic diagram showing the position of wave probes.
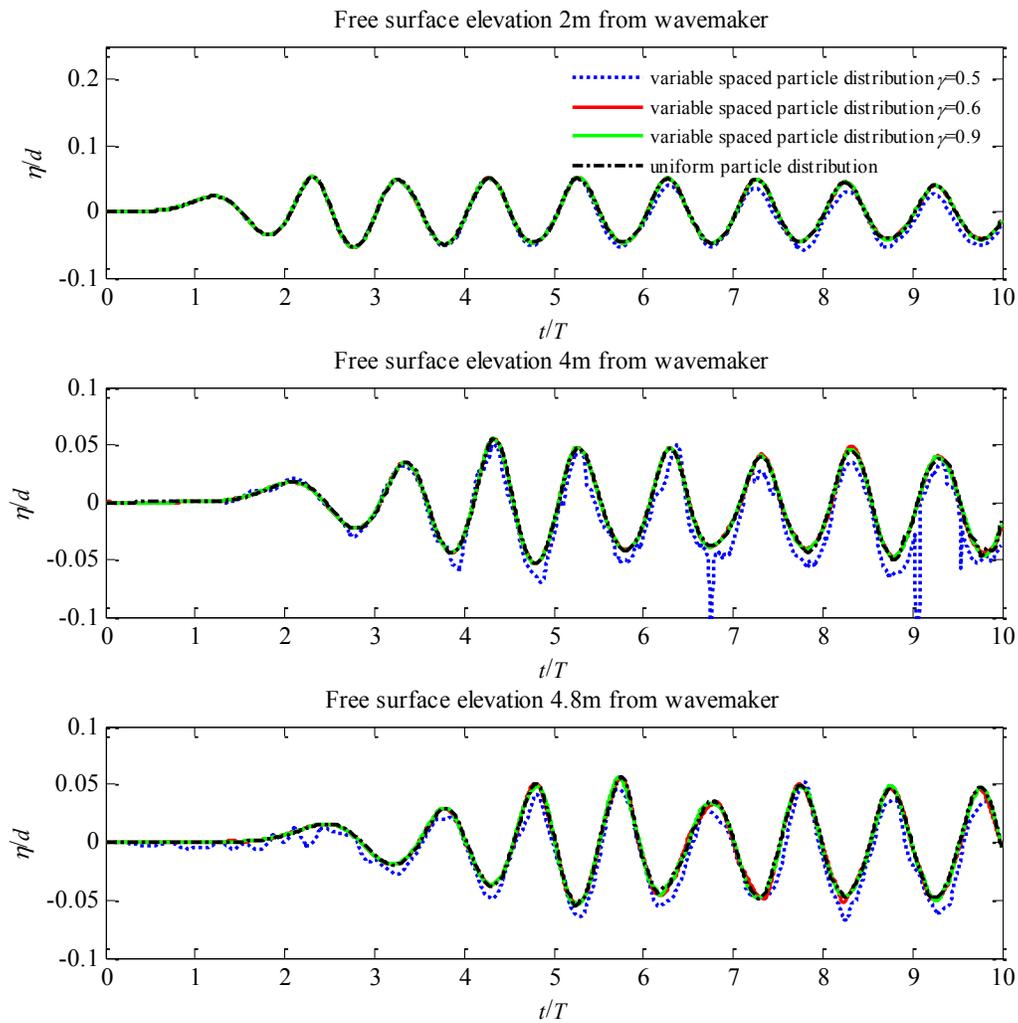
Fig. 13. Comparison of time histories of wave elevation at different locations for different values of γ corresponding to H=0.04m and T=1.2s.
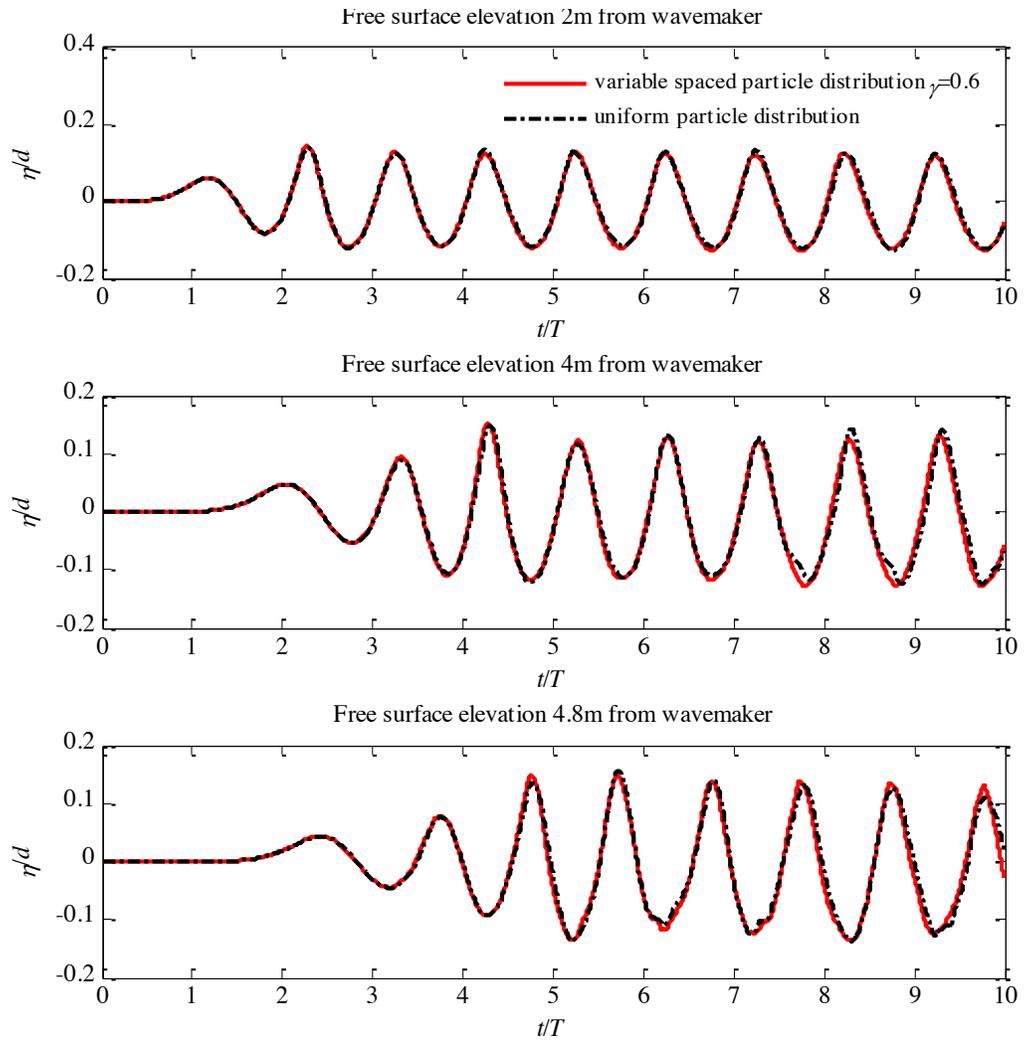
Fig. 14. Comparison of time histories of wave elevation at different locations for different values of γ corresponding to H=0.1m and T=1.2s.
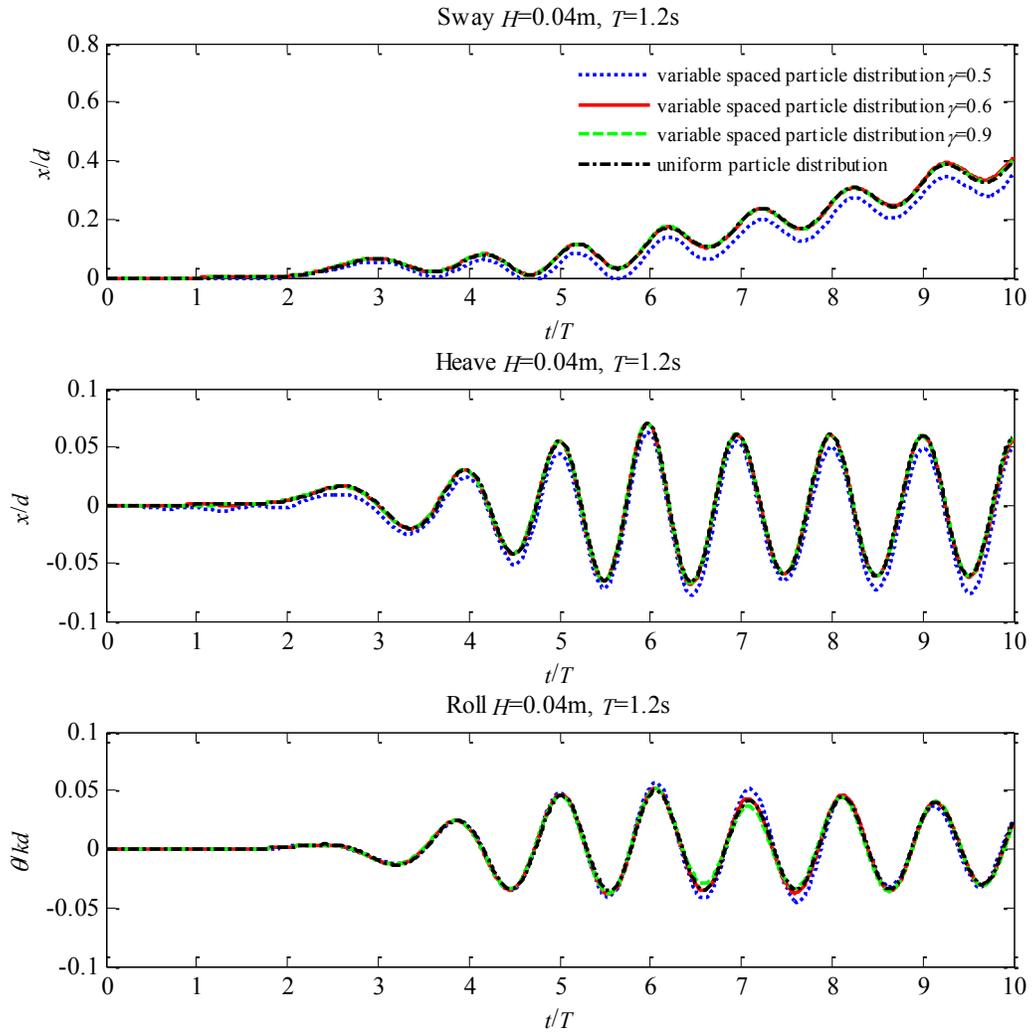
Fig. 15. Comparison of time histories of motion trajectories for different values of γ corresponding to H=0.04m and T=1.2s.
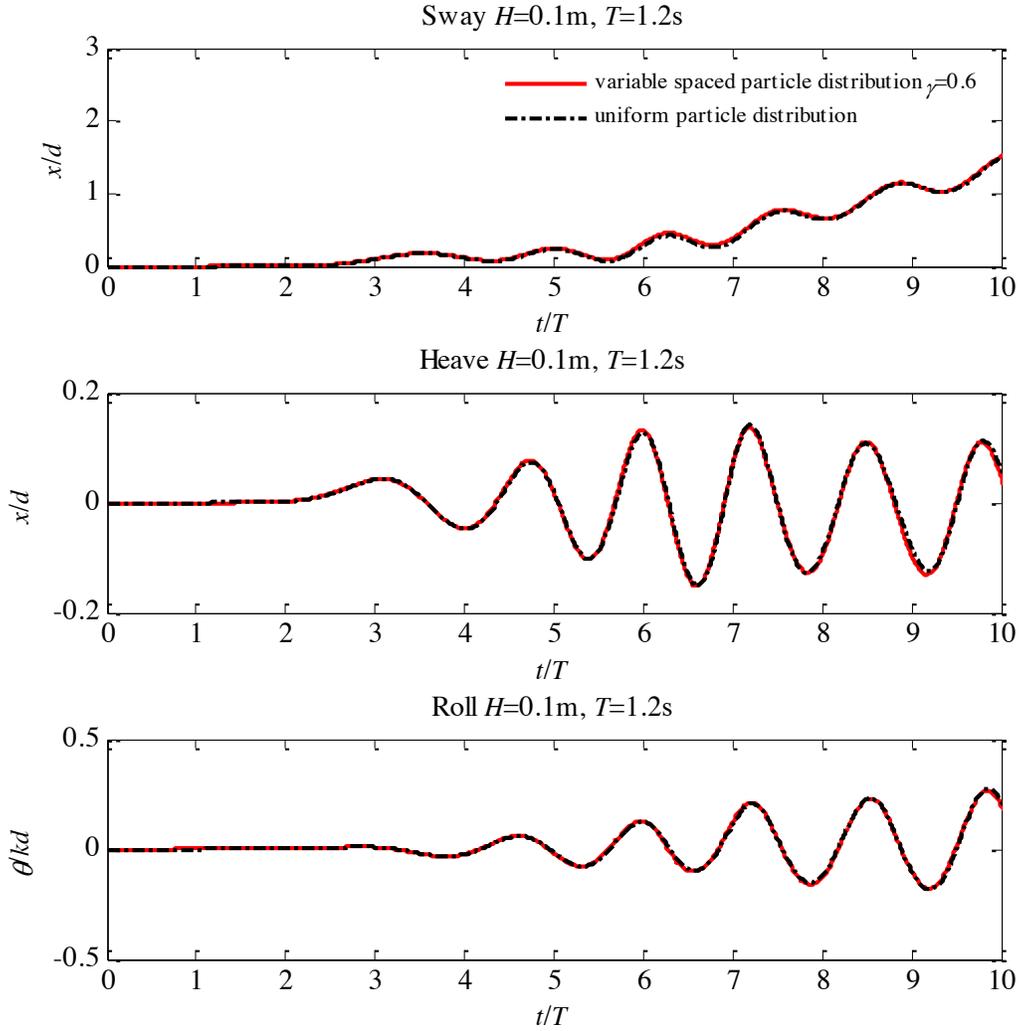
Fig. 16. Comparison of time histories of motion trajectories for different values of γ corresponding to H=0.04m and T=1.2s.
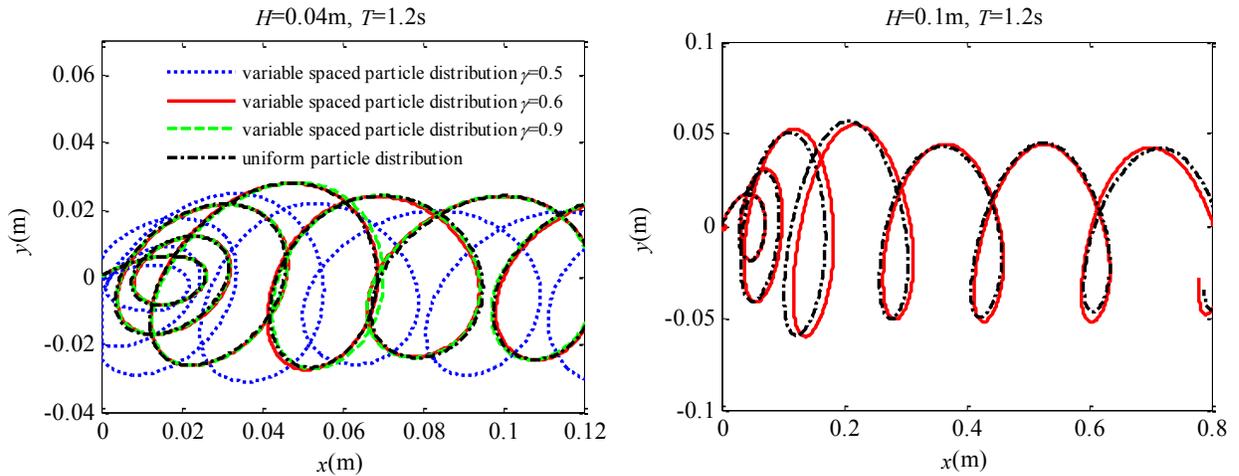
Fig. 17. Comparison of motion trajectories of the centroid of the floating body for different values of γ.
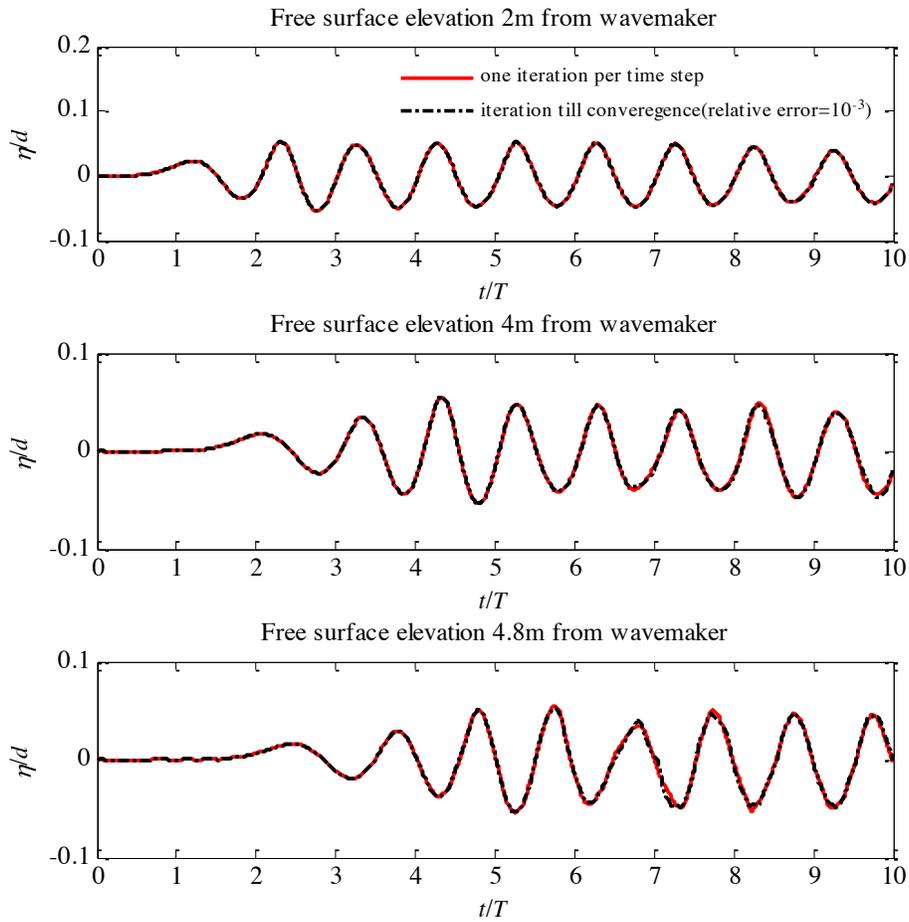
Fig. 18. Comparison of time histories of wave elevation at different locations for a different number of iterations corresponding to H=0.04m and T=1.2s.
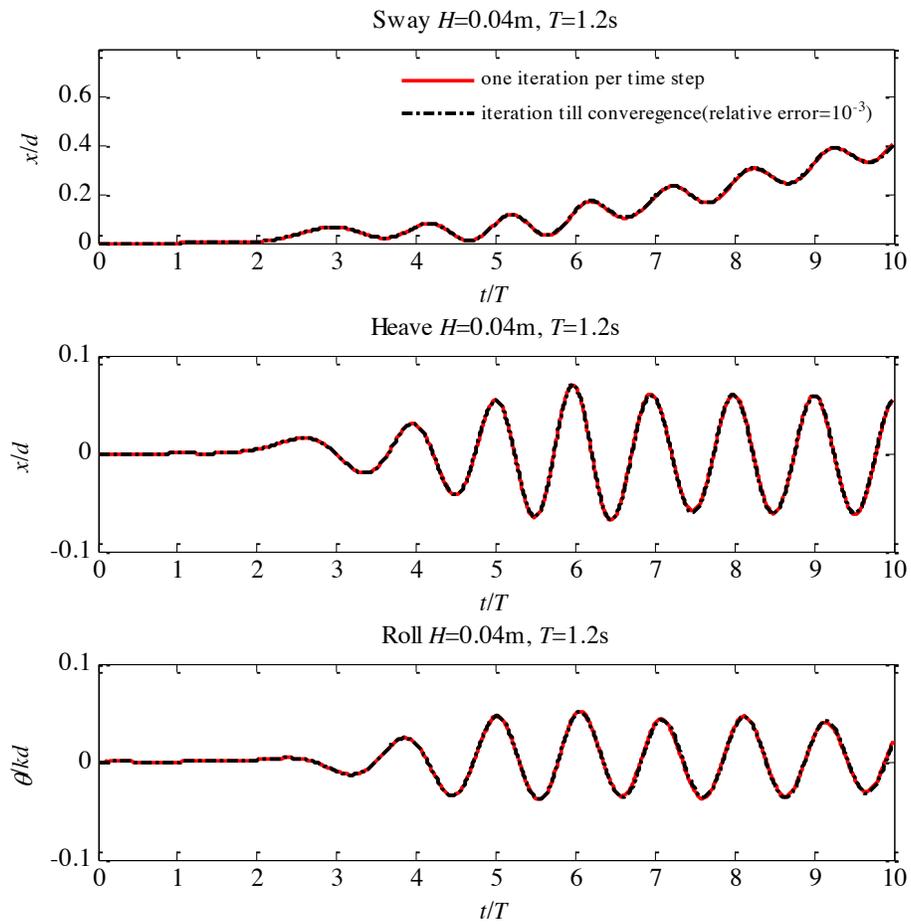
Fig. 19. Comparison of time histories of motion trajectories for a different number of iterations corresponding to *H*=0.04m and *T*=1.2s.
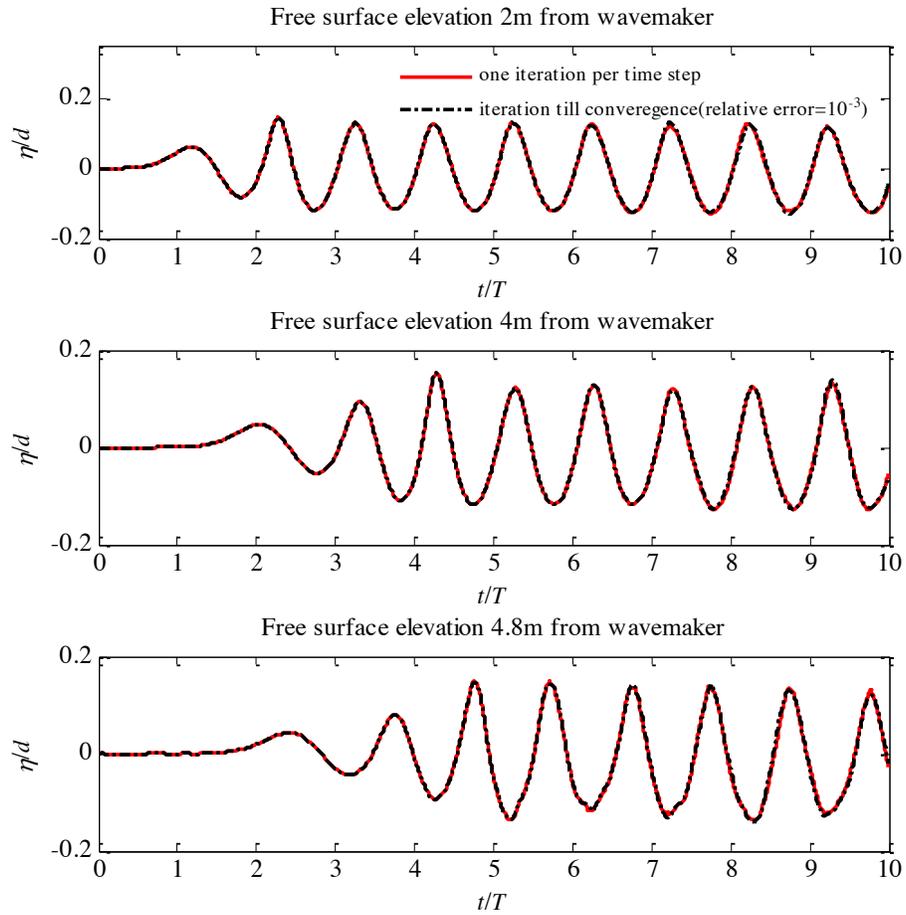
Fig. 20. Comparison of time histories of wave elevation at different locations for different number of iterations corresponding to *H*=0.1m and *T*=1.2s.
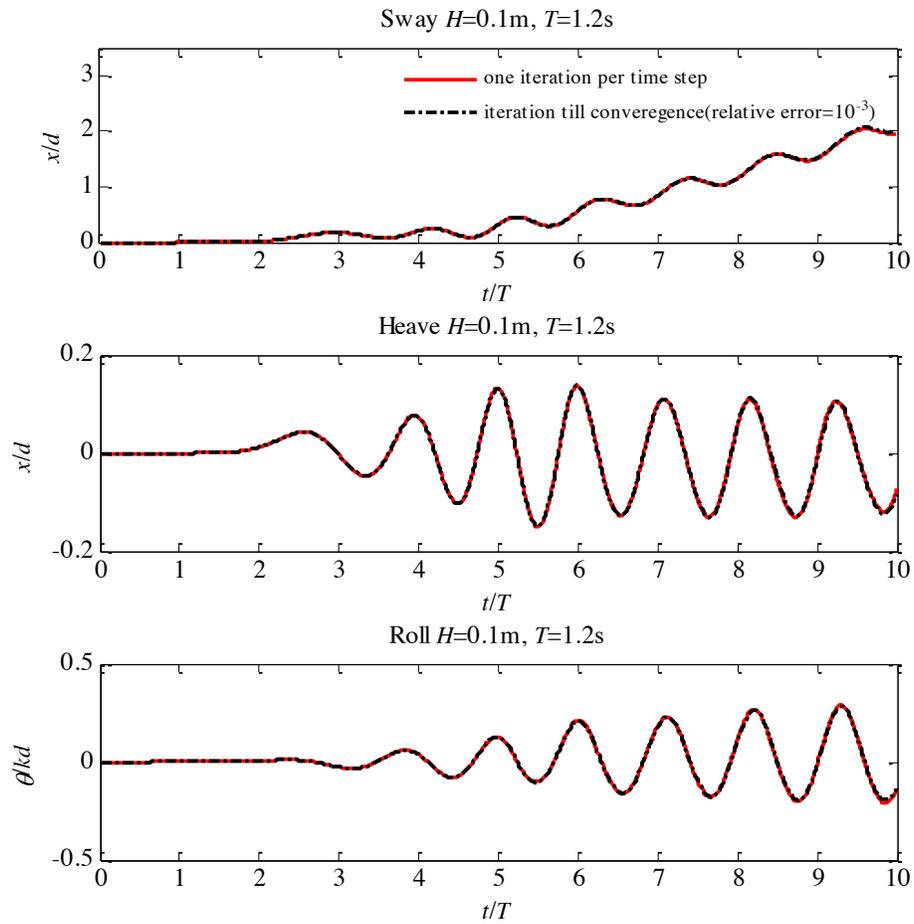
Fig. 21. Comparison of time histories of motion trajectories for a different number of iterations corresponding to *H*=0.04m and *T*=1.2s.
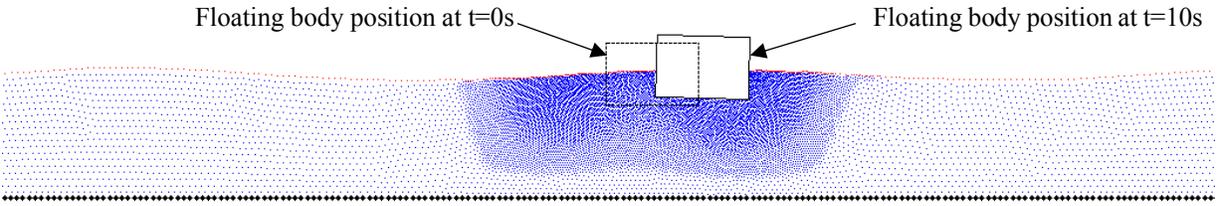
(a)Particle distribution in the domain for H=0.04m and T=1.2s.
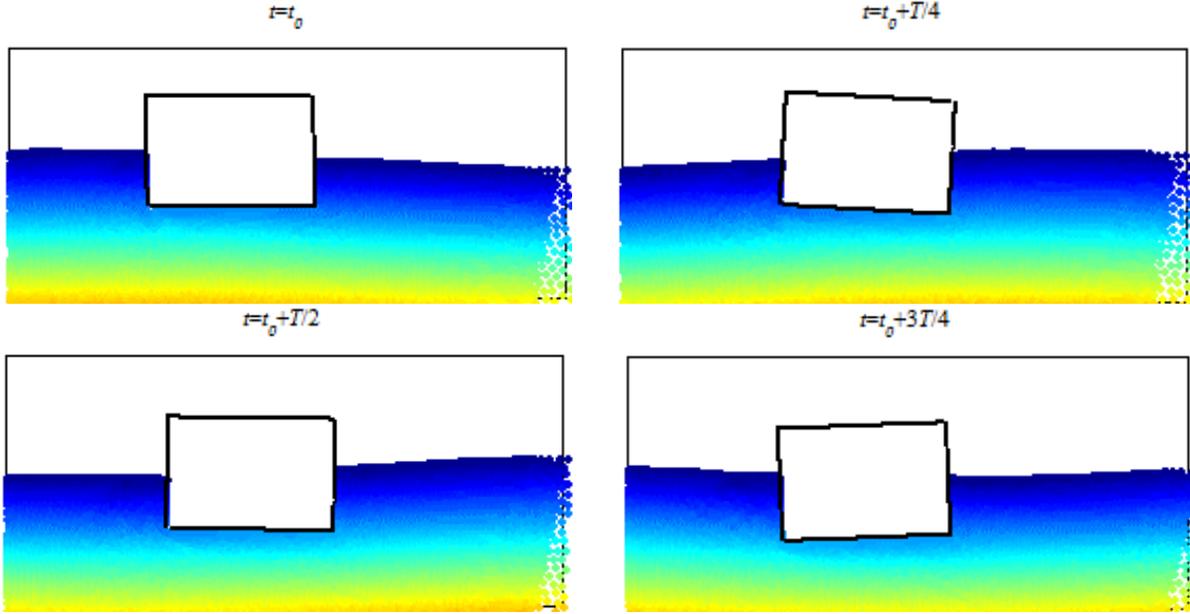
(b) Pressure contour near the body for H=0.04m and T=1.2s.
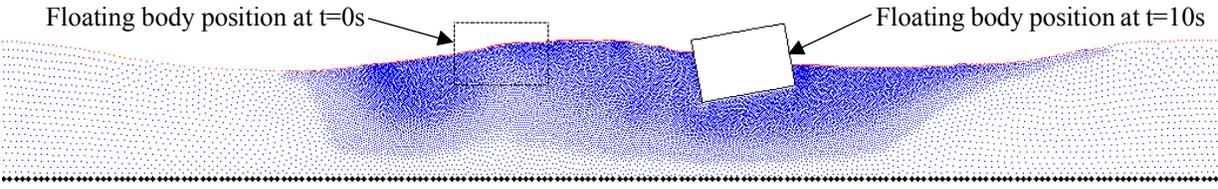
(c)Particle distribution in the domain H=0.1m and T=1.2s.
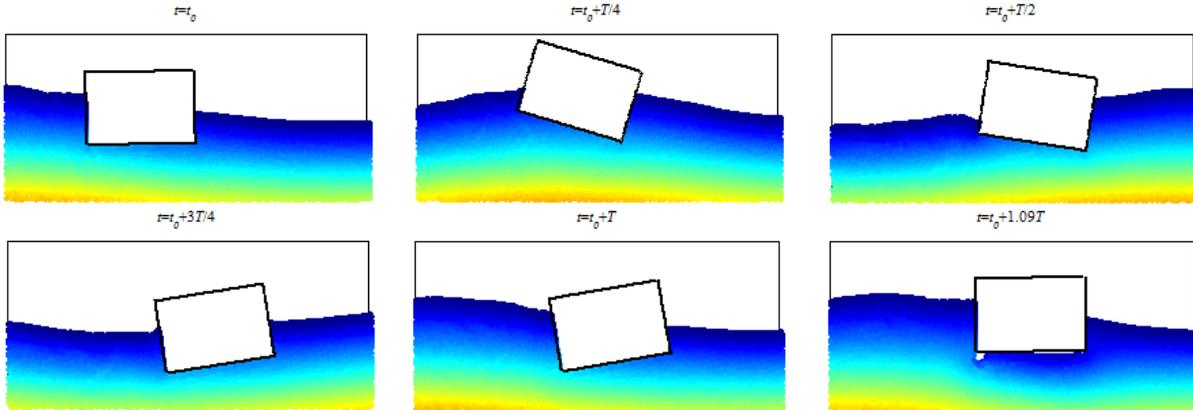
(d) Pressure contour near the body for H=0.1m and T=1.2s.

Fig. 22. Particle distribution and comparison of floating body motion under the wave in different instants of time computed by IMLPG_R method.
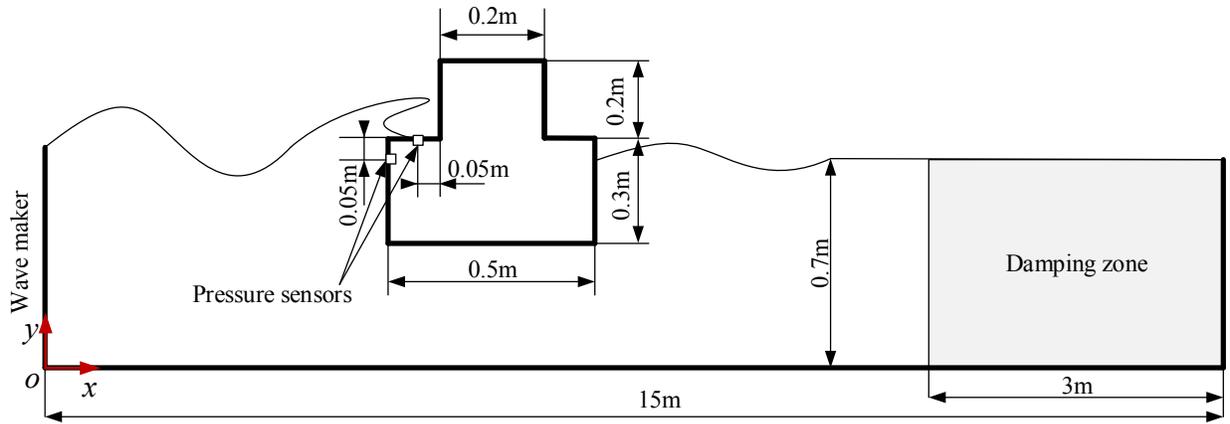
Fig. 23. Schematic diagram for green water impact on the floating structure.
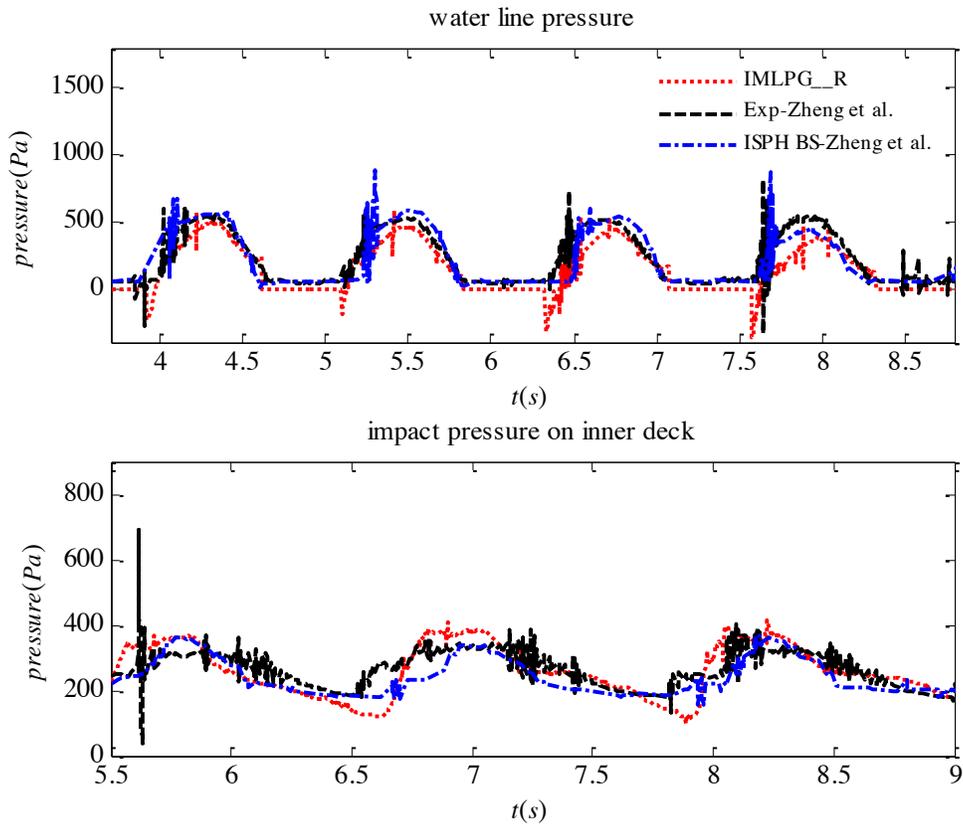
Fig. 24. Time histories of impact pressure at water line and inner deck of the floating body for wave with *H*=0.1m and *T*=1.2s.
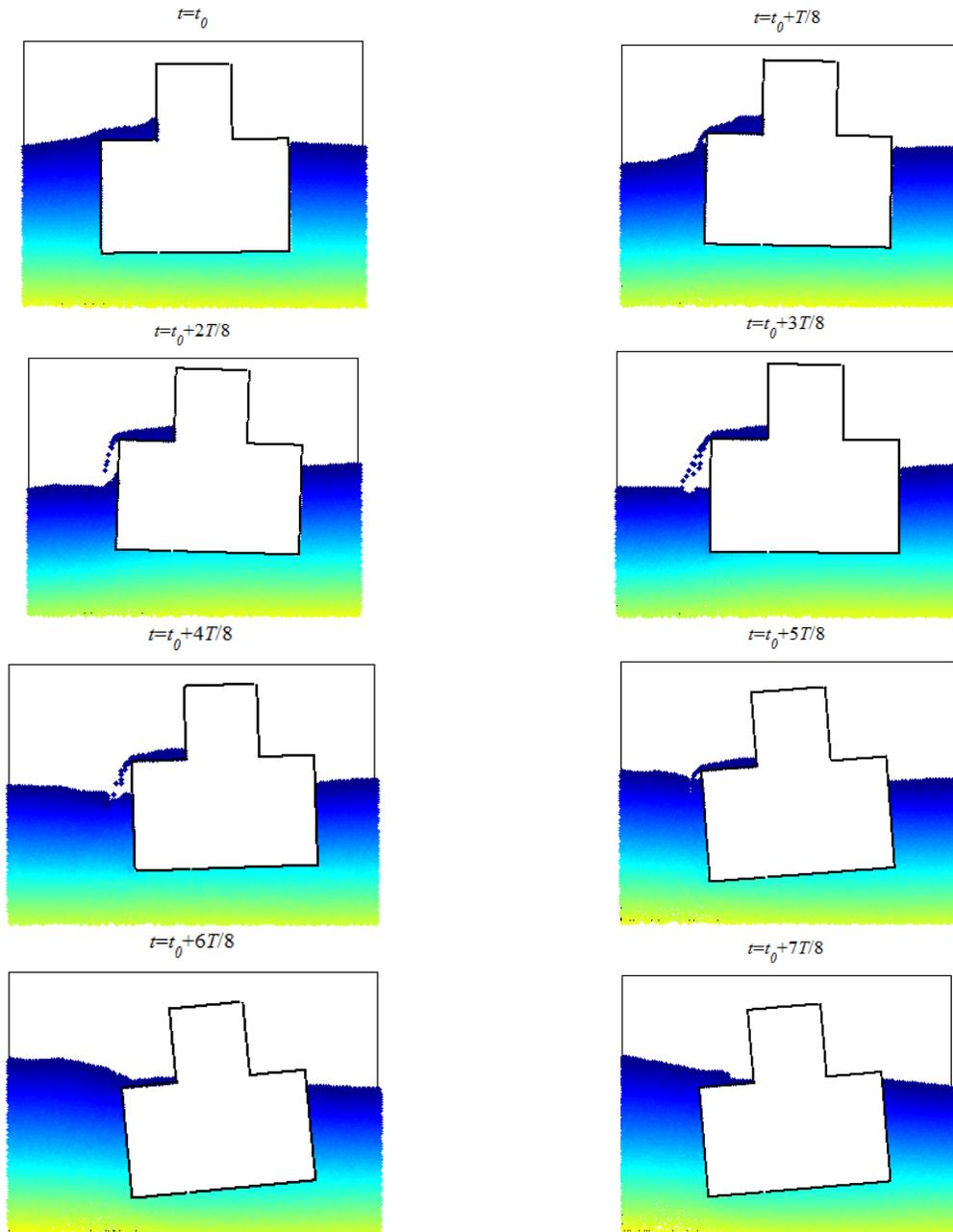
Fig. 25. Comparison of floating body motion under the wave in different instants of time computed by IMLPG_R method.

Table 1. Comparison of computation time with uniform particle distribution and variable spaced particle distribution.

Wave properties	Type of particle distribution	Particle spacing near the floating body	Total number of particles	Computation time(for 10 wave period)
H=0.04m and T=1.2s	Uniform	0.005m	323461	19Hr:50Min
	Variable with γ=0.6	0.005m(near the floating body)to 0.02m(in the far field)	30912	2Hr:46Min
H=0.1m and T=1.2s	Uniform	0.005m	323461	23Hr:21Min
	Variable with γ=0.6	0.005m(near the floating body)to 0.02m(in the far field)	38850	3Hr:7Min

Table 2. Comparison of computation time with one iteration and more iterations till convergence.

Wave properties	No of iterations	Total number of particles	Computation time(for 10 wave period)
H=0.04m and T=1.2s	One iteration	30912	2Hr:46Min
	Till convergence(Relative error=10^{-3})	30912	3Hr:26Min
H=0.1m and T=1.2s	One iteration	38850	3Hr:7Min
	Till convergence(Relative error=10^{-3})	38850	20Hr:38Min